

Fourth Order Positivity and Bound Preserving Well-Balanced Compact Finite Difference Scheme for Ripa and Pollutant Transport Systems

Baifen Ren*, Bao-Shan Wang[†], Xiangxiong Zhang[‡], Zhen Gao[§]

Abstract

We construct a fourth-order accurate compact finite difference scheme that is well-balanced, positivity-preserving of water height, and bound-preserving of concentration for Ripa and pollutant transport systems. The proposed scheme preserves the still-water steady state and the positivity of water height. It also maintains concentration bounds for pollutants across nonflat bottom topographies, regardless of the presence of a pollutant source. Our approach incorporates water height and pollutant concentration constraints within the same discretization, utilizing weak monotonicity and a simple bound-preserving limiter while preserving the well-balanced property. Through extensive numerical simulations encompassing Ripa and pollutant transport models, we demonstrate the effectiveness of our method, verifying its well-balanced property, high-order accuracy, positivity-preserving, and bound-preserving capabilities.

Keywords: Compact finite difference scheme, High order accuracy, Well-balanced, positivity-preserving, bound-preserving, Ripa model, Pollutant transport model.

1 Introduction

In this paper, we consider the system describing the dynamics of flows with the advection equation, which fits both the Ripa model and the pollutant transport model,

$$\frac{\partial \mathbf{Q}}{\partial t} + \nabla \cdot \mathbf{F}(\mathbf{Q}) = \mathbf{S}(\mathbf{Q}, b), \quad (1)$$

*School of Mathematical Sciences, Ocean University of China, Qingdao 266100, China. E-Mail: renbaifen@stu.ouc.edu.cn

[†]School of Mathematical Sciences, Ocean University of China, Qingdao 266100, China. E-Mail: wbs@ouc.edu.cn

[‡]Department of Mathematics, Purdue University, 150 N. University Street, West Lafayette, IN 47907-2067. E-Mail: zhan1966@purdue.edu

[§]Corresponding author. School of Mathematical Sciences, Ocean University of China, Qingdao 266100, China. E-Mail: zhengao@ouc.edu.cn.

where \mathbf{Q} , $\mathbf{F}(\mathbf{Q})$ and $\mathbf{S}(\mathbf{Q}, b)$ are vectors of conservative variables, flux, and source, respectively; with

$$\mathbf{Q} = \begin{pmatrix} h \\ h\mathbf{u} \\ h\xi \end{pmatrix}, \quad \mathbf{F}(\mathbf{Q}) = \begin{pmatrix} h\mathbf{u} \\ h\mathbf{u}^2 + \frac{1}{2}gh^2\phi(\xi)\mathbf{I}_d \\ h\xi\mathbf{u} \end{pmatrix}, \quad \mathbf{S}(\mathbf{Q}, b) = \begin{pmatrix} 0 \\ -gh\phi(\xi)\nabla b \\ 0 \end{pmatrix}, \quad (2)$$

and h is the height of the water, \mathbf{u} is the velocity of the water, g is the gravitational constant, and b represents the bottom topography. The variable ξ and its function $\phi(\xi)$ are given as

$$\xi = \begin{cases} \theta, & \text{Ripa model,} \\ T, & \text{pollutant transport model,} \end{cases} \quad \phi(\xi) = \begin{cases} \theta, & \text{Ripa model,} \\ 1, & \text{pollutant transport model.} \end{cases} \quad (3)$$

In practice, pressure P can be defined by $\frac{1}{2}gh^2\phi(\xi)$. These two models are derived from the shallow water equations by incorporating horizontal temperature or concentration gradients. The first two equations represent the shallow water equations, assuming that the flows exhibit horizontal dimensions significantly greater than their vertical extent. When considering system (1), one can refer to the idea of solving shallow water equations. We refer readers to [31, 32] for shallow water equations. The third equation is an advection equation, which describes the fluctuations in temperature or the transportation of pollution. More details about Ripa model can be found in [23]. The theory of pollutant transportation is introduced in [26]. We refer to [18] for the review of the related (erosion and sediment transport) models.

There are two main challenges in designing a high-order accurate numerical scheme for solving system (2). The first concern is well-balanced property. The model admits the set of stationary solutions

$$h + b = \text{constant}, \quad hu = 0, \quad \text{and} \quad \xi = \text{constant}, \quad (4)$$

that corresponds to a flat water surface with constant temperature in Ripa and pollution concentration in the pollutant transport model. Bermudez and Vazquez [2] firstly proposed the concept of C-property for shallow water equations: a numerical method is said to satisfy this property if it preserves the set of stationary solutions. More generally, a numerical method is considered well-balanced for a given stationary solution if it can accurately capture small perturbations while maintaining the stationary initial conditions, even on a relatively coarse mesh. Concerning the Ripa model, the well-balanced property of different families of numerical methods has been addressed in the literature, such as central-upwind scheme together with an interface tracking method [5], unstaggered central scheme [29], relaxation technique for still water [9], finite difference WENO schemes, space-time CESE scheme [20, 25], discontinuous Galerkin methods for still and moving equilibrium [3], surface reconstruction schemes [10], moving mesh methods [11]. On the other hand, several well-balanced numerical schemes have been developed for pollutant transport model, such as finite element method [14], finite difference WENO scheme [16, 33], flux splitting scheme [30], hybrid finite volume particle method [4].

The second difficulty for approximating system (2) is related to physical constraints including positivity-preserving for water height and bound-preserving for ξ . It's unphysical when non-negative water height and unbound concentration appear. In practice, negative water height and concentration induce the simulation blow-up. One popular methodology to enforce the positivity-preserving

strategy in high-order schemes is to employ a scaling limiter introduced in finite volume and DG schemes [34, 35, 36], which can be proven to have a *weak monotonicity* property, e.g., the cell averages are positive after one forward Euler time stepping. Other strategies can be found in [10, 19]. Both positivity-preserving and well-balanced property have been enforced in [10, 12, 24, 29].

Various high-order numerical schemes have been proposed to address models related to system (2), such as finite difference and finite volume WENO schemes, WCNS and DG methods. The compact finite difference method is a linear scheme [15] that offers advantages, including high-order accuracy, ease of implementation, and compact stencils. Compared to the central scheme, the compact difference method generally offers better stability properties, accuracy with fewer points, and less diffusion, especially for more complex problems. The high-order compact finite scheme is used to solve conservation law in [27]. Additionally, the compact finite difference method has a *weak monotonicity* property, which is an important tool for realizing bound-preserving properties. A bound-preserving compact finite difference scheme has been proposed for scalar convection-diffusion equations in [17]. Its extension to solving shallow water equations has been considered in [22]. The main differences between the application to shallow water model and system (1) are the definition of steady states corresponding to water at rest and the physical constraints of variables. The presence of the variable ξ increases the complexity of these steady states. Besides the challenging shallow water equations, system (1) may contain contact discontinuity in ξ while the pressure is continuous.

In this paper, we propose a well-balanced, positivity-preserving, and bound-preserving fourth-order compact finite difference scheme for solving (1) representing either Ripa or pollution transport model. The key idea in designing a well-balanced scheme is to balance the numerical approximations of source term and flux gradients. To achieve the well-balanced property, we first rewrite the source term to match the effect of flux gradient in the discretization by using the same approach as in [31]. In this article, we apply a nonlinear TVB limiter [6] to realize the nonlinear stability and eliminate oscillations for shocks, which brings extra challenge to designing a well-balanced scheme. Following the approach in [22], the same TVB limiter is used to reconstruct source term and numerical fluxes to preserve well-balancedness. For the positivity and bound preserving property, we will utilize the weak monotonicity of the compact finite difference scheme. We derive suitable CFL conditions for ensuring the weak monotonicity of the compact finite difference scheme when the TVB limiter is used. In particular, the consideration of another variable $h\xi$ will not bring more restrictions on CFL conditions than only enforcing the positivity of water height. With weak monotonicity, a simple limiter can enforce bounds or positivity without affecting high order accuracy. Assuming the cell average value $\bar{h\xi}$ in a 3-point stencil is bounded, the bound-preserving limiter is enforced at first. Then the positivity-preserving limiter is applied based on the positivity of cell average value \bar{h} .

The rest of the paper is organized as follows. A fourth-order well-balanced compact finite difference is provided in Section 2, in which we introduce the numerical reconstructions for flux and bottom topography, as well as TVB limiter. Section 3 introduces the weak monotonicity of the proposed scheme and a simple positivity-preserving limiter that does not affect conservation. With this technique, both the positivity-preserving and bound-preserving properties can be achieved. Section 4 is dedicated to extending the scheme to two-dimensional problems. Numerical experiments related to Ripa and pollutant transport models are given in Section 5 and Section 6, respectively. Section

7 consists of concluding remarks.

2 A fourth-order accurate well-balanced compact finite difference scheme

In this section, firstly, we review the fourth-order compact finite difference scheme. Then, apply it to system (1) and prove the well-balanced property.

If the computation domain is discretized as $[x_0, x_1, \dots, x_N, x_{N+1}]$ with $N + 2$ uniform grid points $x_i = i\Delta x, i = 0, \dots, N + 1$, where $\Delta x = \frac{1}{N+1}$, x_0 and x_{N+1} are nodes at physical boundaries, x_1, \dots, x_N are interior points. For any given smooth function $f(x)$, the combination of first-order derivatives can be approximated by the combination of their function value,

$$\frac{1}{6}(f'(x_{i+1}) + 4f'(x_i) + f'(x_{i-1})) = \frac{f(x_{i+1}) - f(x_{i-1}))}{2\Delta x} + \mathcal{O}(\Delta x^4). \quad (5)$$

For periodic boundary conditions, equation (5) can be reformulated in matrix form,

$$\mathbf{W}\mathbf{f}' = \mathbf{D}\mathbf{f}, \quad (6)$$

where matrices \mathbf{W}, \mathbf{D} , and vectors \mathbf{f}', \mathbf{f} are defined as:

$$\mathbf{W} = \frac{1}{6} \begin{pmatrix} 4 & 1 & & & 1 \\ 1 & 4 & 1 & & \\ & \ddots & \ddots & \ddots & \\ & & 1 & 4 & 1 \\ 1 & & & 1 & 4 \end{pmatrix}, \mathbf{D} = \frac{1}{2\Delta x} \begin{pmatrix} 0 & 1 & & & -1 \\ -1 & 0 & 1 & & \\ & \ddots & \ddots & \ddots & \\ & & -1 & 0 & 1 \\ 1 & & & -1 & 0 \end{pmatrix}, \mathbf{f} = \begin{pmatrix} f_1 \\ f_2 \\ \vdots \\ f_{N-1} \\ f_N \end{pmatrix}, \mathbf{f}' = \begin{pmatrix} f'_1 \\ f'_2 \\ \vdots \\ f'_{N-1} \\ f'_N \end{pmatrix}, \quad (7)$$

System (6) can be solved by

$$\mathbf{f}' = \mathbf{W}^{-1}\mathbf{D}\mathbf{f}, \quad (8)$$

For non-periodic boundary conditions, matrices \mathbf{W}, \mathbf{D} become tridiagonal matrices. The information for derivatives at physical boundaries will be needed and can be approximated as in [15]. Before applying the compact finite difference to Ripa and pollutant transportation equations (1), we reformulate the governing equations in one dimension as:

$$\frac{\partial \mathbf{Q}}{\partial t} + \frac{\partial \mathbf{F}(\mathbf{Q})}{\partial x} = \mathbf{A}\mathbf{B}_x, \quad (9)$$

where

$$\mathbf{Q} = \begin{pmatrix} h \\ hu \\ h\xi \end{pmatrix}, \quad \mathbf{F}(\mathbf{Q}) = \begin{pmatrix} hu \\ hu^2 + \frac{1}{2}gh^2\phi(\xi) - \frac{1}{2}gb^2\phi(\xi) \\ hu\xi \end{pmatrix},$$

$$\mathbf{A} = \begin{pmatrix} 0 & 0 & 0 \\ 0 & -g(h+b)\phi(\xi) & -\frac{1}{2}gb^2\phi'(\xi) \\ 0 & 0 & 0 \end{pmatrix}, \quad \mathbf{B}_x = \begin{pmatrix} 0 \\ b_x \\ \xi_x \end{pmatrix},$$

where the following equality has been taken into account

$$-gh\phi(\xi)b_x = \left(\frac{1}{2}gb^2\phi(\xi)\right)_x - g(h+b)b_x - \frac{1}{2}gb^2\phi'(\xi)\xi_x, \quad (10)$$

which is based on the proposal in [31] for shallow water equation. Note that \mathbf{A} is a constant matrix at still water steady states (4). According to (8), the derivatives in \mathbf{B}_x can be solved by

$$\mathbf{b}_x = \mathbf{W}^{-1}\mathbf{D}\mathbf{b}, \quad \xi_x = \mathbf{W}^{-1}\mathbf{D}\xi. \quad (11)$$

To apply compact finite difference, we multiply both sides of (9) by the matrix \mathbf{W} , according to (5), the first order forward Euler time discretization for equation (9) can be expressed as

$$\overline{\mathbf{Q}}_i^{n+1} = \overline{\mathbf{Q}}_i^n - \frac{\Delta t}{\Delta x} \left(\widehat{\mathbf{F}}_{i+\frac{1}{2}} - \widehat{\mathbf{F}}_{i-\frac{1}{2}} \right) - \frac{\Delta t}{\Delta x} \overline{\mathbf{A}}_i(\mathbf{B}_x)_i, \quad (12)$$

where $\overline{\mathbf{A}}_i = \mathbf{W}\mathbf{A}_i$ and $\overline{\mathbf{Q}}_i$ is a weighted average on a three-point compact stencil given as

$$\overline{\mathbf{Q}}_i = \frac{1}{6}(\mathbf{Q}_{i+1} + 4\mathbf{Q}_i + \mathbf{Q}_{i-1}), \quad (13)$$

and the numerical flux is

$$\widehat{\mathbf{F}}_{i+\frac{1}{2}} = \frac{1}{2}(\mathbf{F}_{i+1}^n + \mathbf{F}_i^n). \quad (14)$$

The equations (12)-(14) are classical compact finite difference schemes, and it is known that there may be oscillations near the discontinuities. To avoid them, a TVB limiter is adopted to handle oscillations as [17], and then the equation (12) becomes

$$\overline{\mathbf{Q}}_i^{n+1} = \overline{\mathbf{Q}}_i^n - \frac{\Delta t}{\Delta x} \left(\widehat{\mathbf{F}}_{i+\frac{1}{2}}^{(m)} - \widehat{\mathbf{F}}_{i-\frac{1}{2}}^{(m)} \right) - \frac{\Delta t}{\Delta x} \overline{\mathbf{A}}_i(\mathbf{B}_x^{(m)})_i, \quad (15)$$

where the superscript (m) denotes limited reconstruction. The reconstruction for $\widehat{\xi}_{i\pm\frac{1}{2}}^{(m)}$ is the same as $\widehat{\mathbf{b}}_{i\pm\frac{1}{2}}^{(m)}$. To save space, we only show $\widehat{\mathbf{F}}_{i+\frac{1}{2}}^{(m)}$, $\widehat{\mathbf{b}}_{i+\frac{1}{2}}^{(m)}$ for example, and $\widehat{\mathbf{F}}_{i-\frac{1}{2}}^{(m)}$, $\widehat{\mathbf{b}}_{i-\frac{1}{2}}^{(m)}$ can be similarly defined by shifting the cell index i as $i-1$. The algorithm to define the limited $\widehat{\mathbf{F}}_{i+\frac{1}{2}}^{(m)}$ and $\widehat{\mathbf{b}}_{i+\frac{1}{2}}^{(m)}$ is as follows.

- Firstly, we use the global Lax-Friedrichs flux splitting [31, 37]

$$\mathbf{F}^\pm(\mathbf{Q}) = \frac{1}{2} \left[\begin{pmatrix} hu \\ hu^2 + \frac{1}{2}gh^2\phi(\xi) - \frac{1}{2}gb^2\phi(\xi) \\ h\xi u \end{pmatrix} \pm \alpha \begin{pmatrix} h+b \\ hu \\ (h+b)\xi \end{pmatrix} \right], \quad (16)$$

where $\alpha = \max(|u| \pm \sqrt{gh\phi(\xi)})$. In particular, the first and third components of the viscous term in LF splitting are modified in a well-balanced manner since $h+b$ and ξ are constants at steady states.

- Secondly, we define the differences between reconstructed fluxes as

$$d\widehat{\mathbf{F}}_{i+\frac{1}{2}}^+ = \widehat{\mathbf{F}}_{i+\frac{1}{2}}^+ - \mathbf{F}^+(\overline{\mathbf{Q}}_i), \quad d\widehat{\mathbf{F}}_{i+\frac{1}{2}}^- = \mathbf{F}^-(\overline{\mathbf{Q}}_{i+1}) - \widehat{\mathbf{F}}_{i+\frac{1}{2}}^-, \quad (17)$$

where

$$\widehat{\mathbf{F}}_{i+\frac{1}{2}}^+ = \frac{1}{2}(\mathbf{F}^+(\mathbf{Q})_{i+1} + \mathbf{F}^+(\mathbf{Q})_i), \quad \widehat{\mathbf{F}}_{i+\frac{1}{2}}^- = \frac{1}{2}(\mathbf{F}^-(\mathbf{Q})_{i+1} + \mathbf{F}^-(\mathbf{Q})_i). \quad (18)$$

- Thirdly, TVB limiter in [6] is defined by the modified *minmod* function on (17) to construct limited variables in a component-wise manner,

$$\begin{aligned} d\widehat{\mathbf{F}}_{i+\frac{1}{2}}^{+(m)} &= \text{MMinMod} \left(d\widehat{\mathbf{F}}_{i+\frac{1}{2}}^+, \Delta^+ \mathbf{F}^+(\overline{\mathbf{Q}}_i), \Delta^+ \mathbf{F}^+(\overline{\mathbf{Q}}_{i-1}) \right), \\ d\widehat{\mathbf{F}}_{i+\frac{1}{2}}^{-(m)} &= \text{MMinMod} \left(d\widehat{\mathbf{F}}_{i+\frac{1}{2}}^-, \Delta^+ \mathbf{F}^-(\overline{\mathbf{Q}}_i), \Delta^+ \mathbf{F}^-(\overline{\mathbf{Q}}_{i+1}) \right), \end{aligned} \quad (19)$$

where $\Delta^+ v_i \equiv v_{i+1} - v_i$ is the usual forward difference operator, and modified *minmod* function [27] is defined by

$$\text{MMinMod}(a_1, \dots, a_k) = \begin{cases} a_1, & \text{if } |a_1| \leq \gamma \Delta x^2, \\ \text{MinMod}(a_1, \dots, a_k) & \text{otherwise,} \end{cases} \quad (20)$$

with γ being a positive constant independent of Δx and the *minmod* function is

$$\text{MinMod}(a_1, \dots, a_k) = \begin{cases} s \min_{1 \leq i \leq k} |a_i|, & \text{if } \text{sign}(a_1) = \dots = \text{sign}(a_k) = s, \\ 0, & \text{otherwise.} \end{cases} \quad (21)$$

Remark 1. *Those differences defined in (19) are upwind biased. The first difference would have more opportunity to be chosen with parameter γ increasing. When parameter γ is big enough to select the first difference, the scheme (15) will be equal to standard compact finite difference (12). In addition, It won't destroy the weak monotonicity proved in Section 3 under suitable CFL conditions. The detailed TVB property can be found in [27].*

- Fourthly, the reconstructed numerical fluxes with TVB limiter are constructed by the sum of positive and negative parts,

$$\widehat{\mathbf{F}}_{i+\frac{1}{2}}^{(m)} = \widehat{\mathbf{F}}_{i+\frac{1}{2}}^{+(m)} + \widehat{\mathbf{F}}_{i+\frac{1}{2}}^{-(m)}, \quad \widehat{\mathbf{F}}_{i+\frac{1}{2}}^{+(m)} = \mathbf{F}^+(\overline{\mathbf{Q}}_i) + d\widehat{\mathbf{F}}_{i+\frac{1}{2}}^{+(m)}, \quad \widehat{\mathbf{F}}_{i+\frac{1}{2}}^{-(m)} = \mathbf{F}^-(\overline{\mathbf{Q}}_{i+1}) - d\widehat{\mathbf{F}}_{i+\frac{1}{2}}^{-(m)}. \quad (22)$$

- Fifthly, we reconstruct $\widehat{\mathbf{b}}_{i+\frac{1}{2}}^{(m)}$ mimicking (19)-(22), we define $\mathbf{b}^\pm = \frac{\mathbf{b}}{2}$, $\widehat{\mathbf{b}}_{i\pm\frac{1}{2}}^\pm = \frac{1}{2}(\mathbf{b}_{i+1}^\pm + \mathbf{b}_i^\pm)$, and $d\widehat{\mathbf{b}}_{i+\frac{1}{2}}^+ = \widehat{\mathbf{b}}_{i+\frac{1}{2}}^+ - \mathbf{b}_i^+$, $d\widehat{\mathbf{b}}_{i+\frac{1}{2}}^- = \mathbf{b}_{i+1}^- - \widehat{\mathbf{b}}_{i+\frac{1}{2}}^-$.

The limiting for $d\widehat{\mathbf{b}}_{i+\frac{1}{2}}^{+(m)}$ is consistent with the choice of $d\widehat{\mathbf{F}}_{i+\frac{1}{2}}^{+(m)}$ which is the second flux in $d\widehat{\mathbf{F}}_{i+\frac{1}{2}}^{+(m)}$ and defined by

$$d\widehat{\mathbf{b}}_{i+\frac{1}{2}}^{+(m)} = \begin{cases} 0, & \text{if } d\widehat{\mathbf{F}}_{i+\frac{1}{2}}^{+(m)} = 0, \\ d\widehat{\mathbf{b}}_{i+\frac{1}{2}}^+, & \text{if } d\widehat{\mathbf{F}}_{i+\frac{1}{2}}^{+(m)} = d\widehat{\mathbf{F}}_{i+\frac{1}{2}}^+, \\ \Delta^+ \mathbf{b}_i^+, & \text{if } d\widehat{\mathbf{F}}_{i+\frac{1}{2}}^{+(m)} = \Delta^+ \mathbf{F}^+((\overline{hu})_i), \\ \Delta^+ \mathbf{b}_{i-1}^+, & \text{if } d\widehat{\mathbf{F}}_{i+\frac{1}{2}}^{+(m)} = \Delta^+ \mathbf{F}^+((\overline{hu})_{i-1}). \end{cases} \quad (23)$$

The limiting for $d\widehat{\mathbf{b}}_{i+\frac{1}{2}}^{-(m)}$ is defined in a similar manner. The limited bottom topography can be defined by

$$\widehat{\mathbf{b}}_{i+\frac{1}{2}}^{(m)} = \widehat{\mathbf{b}}_{i+\frac{1}{2}}^{+(m)} + \widehat{\mathbf{b}}_{i+\frac{1}{2}}^{-(m)}, \quad \widehat{\mathbf{b}}_{i+\frac{1}{2}}^{+(m)} = \mathbf{b}_i^+ + d\widehat{\mathbf{b}}_{i+\frac{1}{2}}^{+(m)}, \quad \widehat{\mathbf{b}}_{i+\frac{1}{2}}^{-(m)} = \mathbf{b}_{i+1}^- - d\widehat{\mathbf{b}}_{i+\frac{1}{2}}^{-(m)}.$$

We denote

$$D_1(\mathbf{F}_i) = \frac{1}{\Delta x} \left(\widehat{\mathbf{F}}_{i+\frac{1}{2}}^{(m)} - \widehat{\mathbf{F}}_{i-\frac{1}{2}}^{(m)} \right), \quad D_2(\mathbf{b}_i) = \frac{1}{\Delta x} \left(\widehat{\mathbf{b}}_{i+\frac{1}{2}}^{(m)} - \widehat{\mathbf{b}}_{i-\frac{1}{2}}^{(m)} \right), \quad \mathbf{b}_x^{(m)} = \mathbf{W}^{-1} D_2(\mathbf{b}), \quad (24)$$

The second equation in (15) writes as follows:

$$(\overline{hu})_i^{n+1} = (\overline{hu})_i^n - \Delta t D_1(F_i) - \Delta t g \overline{[(h+b)\phi(\xi)]}_i (b_x^{(m)})_i - \Delta t \frac{1}{2} g \overline{[b^2\phi'(\xi)]}_i (\xi_x^{(m)})_i, \quad (25)$$

where

$$\overline{[(h+b)\phi(\xi)]}_i = \frac{1}{6} (h_{i+1} + b_{i+1}) \phi(\xi_{i+1}) + \frac{4}{6} (h_i + b_i) \phi(\xi_i) + \frac{1}{6} (h_{i-1} + b_{i-1}) \phi(\xi_{i-1}),$$

and $\overline{[b^2\phi'(\xi)]}_i$ can be given similarly. We have now finished the spatial discretization in (15). The next step is to prove the well-balanced property of the proposed compact scheme. Under the hypothesis of still water steady state (4), the well-balanced property holds for the first (h) and third ($h\xi$) equations, as both flux and source term are zero with $u = 0$. To prove the well-balanced property of the second (hu) equation, since for ‘water at rest’ steady state $h_i + b_i = \text{constant}$, $\xi_i = \text{constant}$ and $\phi'(\xi) = 0$ for all i , the equation (25) can be equivalently written as

$$(\overline{hu})_i^{n+1} = (\overline{hu})_i^n - \Delta t (D_1(F_i) - g (h_i + b_i) \phi(\xi_i) D_2(b_i)). \quad (26)$$

Since the limited reconstruction of the bottom (23) is consistent with that of flux, the non-linear operator with minmod limiter, D_1 and D_2 satisfy the relation $D_1 = D_2 = D$, and

$$\begin{aligned} & D_1 \left(\left(\frac{1}{2} g h^2 - \frac{1}{2} g b^2 \right) \phi(\xi) \right) + g (h + b) \phi(\xi) D_2(b) \\ &= D \left(\left(\frac{1}{2} g h^2 - \frac{1}{2} g b^2 + g (h + b) b \right) \phi(\xi) \right) = D \left(\frac{1}{2} g (h + b)^2 \phi(\xi) \right) = 0. \end{aligned}$$

Therefore, $(\overline{hu})_i^{n+1} = (\overline{hu})_i^n = \dots = (\overline{hu})_i^0$. The proposed compact scheme (15) is well-balanced.

Remark 2. While the computation of ξ_x does not influence the well-balanced property, we adopt the same approach for calculating ξ_x as for b_x to ensure high-order accuracy and suppress oscillations.

3 Positivity and bound preserving property

In this section, we consider the positivity and bound-preserving property of the scheme in Section 2. We check the weak monotonicity of water height h and discuss the property of variable $h\xi$ under appropriate CFL conditions. Since the positivity-preserving limiter is the special case of the bound-preserving limiter, we only describe the algorithm of bound-preserving limiter.

3.1 Weak monotonicity of the compact finite difference scheme

For simplicity, we consider point values under periodic boundary conditions $Q_0 = Q_N, Q_{N+1} = Q_1$. Define $\bar{\mathbf{h}} = \mathbf{Wh}$, i.e., $\bar{h}_i = \frac{1}{6}(h_{i-1} + 4h_i + h_{i+1})$. Then \bar{h}_i represents the cell average of a cubic approximation polynomial within the cell $[x_{i-1}, x_{i+1}]$, see [17]. The fourth-order compact finite difference with the forward Euler time discretization without TVB limiter for the water height equation can be written as

$$\bar{h}_i^{n+1} = \bar{h}_i^n - \frac{\Delta t}{2\Delta x} ((hu)_{i+1}^n - (hu)_{i-1}^n), \quad (27)$$

which is equivalent to the first equation in (12) with (14). Let $\lambda = \frac{\Delta t}{\Delta x}$, then (27) can be reformulated as the convex combination, under the CFL condition $\lambda \max_i |u_i| \leq \frac{1}{3}$,

$$\begin{aligned} \bar{h}_i^{n+1} &= \frac{1}{6} (h_{i-1}^n + 4h_i^n + h_{i+1}^n) - \frac{1}{2}\lambda ((hu)_{i+1}^n - (hu)_{i-1}^n) \\ &= \frac{1}{6}h_{i-1}^n (1 + 3\lambda u_{i-1}^n) + \frac{4}{6}h_i^n + \frac{1}{6}h_{i+1}^n (1 - 3\lambda u_{i+1}^n) \\ &= H(h_{i-1}^n, h_i^n, h_{i+1}^n). \end{aligned} \quad (28)$$

The function H is increasing with respect to each argument $H(\uparrow, \uparrow, \uparrow)$, i.e., the weak monotonicity property of the scheme. Therefore, one has $\bar{h}_i^{n+1} \geq 0$ if $h_i^n \geq 0$ for all i .

As proved in Theorem 2.9 in [17], the conservative scheme (15) with TVB limiter still satisfies $\bar{h}_i^{n+1} \geq 0$ if $h_i^n \geq 0$ under the CFL condition

$$\lambda \max_i |u_i| \leq \frac{1}{12}. \quad (29)$$

The monotonicity of $(\bar{h\xi})_i$ can be deduced from the following equation,

$$\begin{aligned} (\bar{h\xi})_i^{n+1} &= (\bar{h\xi})_i^n - \frac{\Delta t}{2\Delta x} ((h\xi u)_{i+1}^n - (h\xi u)_{i-1}^n) \\ &= \frac{1}{6} ((h\xi)_{i-1}^n + 4(h\xi)_i^n + (h\xi)_{i+1}^n) - \frac{1}{2}\lambda ((h\xi u)_{i+1}^n - (h\xi u)_{i-1}^n) \\ &= \frac{1}{6}(h\xi)_{i-1}^n (1 + 3\lambda u_{i-1}^n) + \frac{4}{6}(h\xi)_i^n + \frac{1}{6}(h\xi)_{i+1}^n (1 - 3\lambda u_{i+1}^n) \\ &= H((h\xi)_{i-1}^n, (h\xi)_i^n, (h\xi)_{i+1}^n) = H(\uparrow, \uparrow, \uparrow), \end{aligned} \quad (30)$$

which means if $m = H(m, m, m) \leq (\bar{h\xi})_i^n \leq H(M, M, M) = M$, then $(\bar{h\xi})_i^{n+1}$ is also bounded in $[m, M]$ with the same CFL condition (29).

Based on the weak monotonicity, a positivity and bound preserving limiter, which will be described in the next subsection, can be applied, to ensure that $h_i^{n+1} \geq 0$ and $(h\xi)_i^{n+1}$ is bounded. We first apply the bound-preserving limiter, then the positivity-preserving limiter follows if necessary. It satisfies the requirement of bound preserving limiter only in this order. Otherwise, the condition

for bound-preserving limiter may not be fulfilled if h is updated. The desingularization formula [13] is utilized to avoid division by a very small value of the water depth:

$$\xi_i = \begin{cases} \frac{(h\xi)_i}{h_i}, & \text{if } h_i > 10^{-6}, \\ \min\{\xi_{\max}, \max\{\xi_{\min}, R_i\}\}, & \text{otherwise,} \end{cases} \quad R_i = \frac{\sqrt{2}h_i(h\xi)_i}{\sqrt{h_i^4 + \max(h_i^4, (\Delta x)^4)}}.$$

3.2 A simple positivity and bound preserving limiter

The 3-point stencil cell-averages $\bar{h}_i^{n+1}, (\bar{h\xi})_i^{n+1}$ will be positive and bounded by scheme (15). And point values $h_i^{n+1}, (h\xi)_i^{n+1}$ is computed by solving the system $\mathbf{W}Q^{n+1} = \bar{Q}^{n+1}$. Then $h_i^{n+1}, (h\xi)_i^{n+1}$ are enforced to be positive and bounded respectively by applying the bound-preserving limiter in Algorithm 1.

The bound-preserving limiter does not rely on the boundary conditions. For simplicity, we consider point values $Q_i, i = 1, \dots, N$ satisfying $m \leq \bar{Q}_i \leq M$ for $i = 1, \dots, N$ under periodic boundary conditions $Q_0 = Q_N, Q_{N+1} = Q_1$. For the water height positivity-preserving property, we only consider the lower bound with $m = 0, M = +\infty$; for the variable $h\xi$, both the lower and upper bounds are required.

Algorithm 1 A bound-preserving limiter.

Require: the input d_i satisfies $\bar{d}_i = \frac{1}{6}(d_{i-1} + 4d_i + d_{i+1}) \in [m, M]$. Let d_0, d_{N+1} denote d_N, d_1 , respectively.

Ensure: the output satisfies $s_i \in [m, M], i = 1, \dots, N$ and $\sum_{i=1}^N s_i = \sum_{i=1}^N d_i$.

- 1: First set $s_i = d_i, i = 1, \dots, N$. Let s_0, s_{N+1} denote s_N, s_1 , respectively.
 - 2: **for** all index $i = 1, \dots, N$ **do**
 - 3: **if** $d_i < m$ **then**
 - 4: $s_{i-1} \leftarrow s_{i-1} - \frac{(d_{i-1}-m)_+}{(d_{i-1}-m)_+ + (d_{i+1}-m)_+} (m - d_i)_+$
 - $s_{i+1} \leftarrow s_{i+1} - \frac{(d_{i+1}-m)_+}{(d_{i-1}-m)_+ + (d_{i+1}-m)_+} (m - d_i)_+$
 - $s_i \leftarrow m$
 - 5: **end if**
 - 6: **if** $d_i > M$ **then**
 - 7: $s_{i-1} \leftarrow s_{i-1} + \frac{(M-d_{i-1})_+}{(M-d_{i-1})_+ + (M-d_{i+1})_+} (d_i - M)_+$
 - $s_{i+1} \leftarrow s_{i+1} + \frac{(M-d_{i+1})_+}{(M-d_{i-1})_+ + (M-d_{i+1})_+} (d_i - M)_+$
 - $s_i \leftarrow M$
 - 8: **end if**
 - 9: **end for**
-

The subscript $+$ in Algorithm 1 denotes the positive part, i.e., $(a)_+ = \max\{a, 0\}$. The limiter is based on the local operation, and only those trouble points and its immediate neighboring points are

modified. The limiter can enforce bounds of point values without affecting global conservation and high order accuracy [17]. The limiter will not be activated if all point values are already bounded. Notice that neither bound-preserving nor positivity-preserving limiter will be triggered for a still-water steady state, thus the well-balanced property is not affected by Algorithm 1.

3.3 Higher order time discretizations

In this paper, third order SSP Runge-Kutta method [28] which is a convex combination of three forward Euler steps (15) will be used as the time discretization.

Since bound and positivity are preserved by a convex combination, SSP Runge-Kutta, with the simple limiter Algorithm 1 used in each time step, is still positivity and bound preserving under a suitable CFL condition. Each SSP Runge-Kutta method has a stability coefficient $c_s > 0$. For the third order SSP Runge-Kutta method, $c_s = \frac{1}{3}$, which means that the fully discrete scheme using SSP Runge-Kutta method and Algorithm 1 preserve bounds under the CFL condition

$$\lambda \max_i |u_i| \leq c_s \frac{1}{12} = \frac{1}{36}. \quad (31)$$

Notice that the CFL condition is a sufficient rather than necessary condition for achieving bounds and positivity. Thus, in practice, one can enforce such a small CFL condition only when positivity and bounds are lost; see [34] for such an implementation.

4 Extension to two dimensions

In this section, we extend the proposed scheme from the 1D to 2D case in a dimension-by-dimension fashion. The governing equations with two-dimensional models are given by:

$$\frac{\partial \mathbf{Q}}{\partial t} + \mathbf{F}(\mathbf{Q})_x + \mathbf{G}(\mathbf{Q})_y = \mathbf{A}^x \mathbf{B}_x + \mathbf{A}^y \mathbf{B}_y, \quad (32)$$

where \mathbf{Q} , $\mathbf{F}(\mathbf{Q})$, and $\mathbf{G}(\mathbf{Q})$ are

$$\mathbf{Q} = \begin{pmatrix} h \\ hu \\ hv \\ h\xi \end{pmatrix}, \quad \mathbf{F}(\mathbf{Q}) = \begin{pmatrix} hu \\ hu^2 + \frac{1}{2}g\phi(\xi)h^2 - \frac{1}{2}g\phi(\xi)b^2 \\ huv \\ hu\xi \end{pmatrix}, \quad \mathbf{G}(\mathbf{Q}) = \begin{pmatrix} hv \\ huv \\ hv^2 + \frac{1}{2}g\phi(\xi)h^2 - \frac{1}{2}g\phi(\xi)b^2 \\ hv\xi \end{pmatrix}, \quad (33)$$

respectively, and source terms matrices in x, y direction read

$$\mathbf{A}^x = \begin{pmatrix} 0 & 0 & 0 & 0 \\ 0 & -g(h+b)\phi(\xi) & -\frac{1}{2}gb^2\phi'(\xi) & 0 \\ 0 & 0 & 0 & 0 \\ 0 & 0 & 0 & 0 \end{pmatrix}, \quad \mathbf{B}_x = \begin{pmatrix} 0 \\ b_x \\ \xi_x \\ 0 \end{pmatrix},$$

$$\mathbf{A}^y = \begin{pmatrix} 0 & 0 & 0 & 0 \\ 0 & 0 & 0 & 0 \\ 0 & 0 & -g(h+b)\phi(\xi) & -\frac{1}{2}gb^2\phi'(\xi) \\ 0 & 0 & 0 & 0 \end{pmatrix}, \quad \mathbf{B}_y = \begin{pmatrix} 0 \\ 0 \\ b_y \\ \xi_y \end{pmatrix}.$$

For simplicity, we discuss the fourth order compact finite difference scheme with $N_x \times N_y$ uniform grid points with periodic boundary conditions.

We define $\widehat{\mathbf{F}}, \widehat{\mathbf{G}}, \widehat{\mathbf{b}}$ as

$$\begin{aligned} \widehat{\mathbf{F}}_{i+\frac{1}{2},j} &= \frac{1}{2}(\mathbf{F}_{i+1,j}^n + \mathbf{F}_{i,j}^n), & \widehat{\mathbf{G}}_{i,j+\frac{1}{2}} &= \frac{1}{2}(\mathbf{G}_{i,j+1}^n + \mathbf{G}_{i,j}^n), \\ \widehat{\mathbf{b}}_{i+\frac{1}{2},j} &= \frac{1}{2}(\mathbf{b}_{i+1,j}^n + \mathbf{b}_{i,j}^n), & \widehat{\mathbf{b}}_{i,j+\frac{1}{2}} &= \frac{1}{2}(\mathbf{b}_{i,j+1}^n + \mathbf{b}_{i,j}^n). \end{aligned} \quad (34)$$

W_x and W_y are two linear operators, from $R^{N_x \times N_y}$ to $R^{N_x \times N_y}$:

$$\begin{aligned} W_x \mathbf{f} &= \frac{1}{6} \begin{pmatrix} 4 & 1 & & 1 \\ 1 & 4 & 1 & \\ & \ddots & \ddots & \ddots \\ & & 1 & 4 & 1 \\ 1 & & & 1 & 4 \end{pmatrix}_{N_x \times N_x} \begin{pmatrix} f_{11} & f_{12} & \cdots & f_{1N_y} \\ f_{21} & f_{22} & \cdots & f_{2N_y} \\ \vdots & \vdots & \ddots & \vdots \\ f_{N_x-1,1} & f_{N_x-1,2} & \cdots & f_{N_x-1,N_y} \\ f_{N_x,1} & f_{N_x,2} & \cdots & f_{N_x,N_y} \end{pmatrix}, \\ W_y \mathbf{f} &= \begin{pmatrix} f_{11} & f_{12} & \cdots & f_{1N_y} \\ f_{21} & f_{22} & \cdots & f_{2N_y} \\ \vdots & \vdots & \ddots & \vdots \\ f_{N_x-1,1} & f_{N_x-1,2} & \cdots & f_{N_x-1,N_y} \\ f_{N_x,1} & f_{N_x,2} & \cdots & f_{N_x,N_y} \end{pmatrix} \frac{1}{6} \begin{pmatrix} 4 & 1 & & 1 \\ 1 & 4 & 1 & \\ & \ddots & \ddots & \ddots \\ & & 1 & 4 & 1 \\ 1 & & & 1 & 4 \end{pmatrix}_{N_y \times N_y}. \end{aligned}$$

D_x and D_y are difference operators:

$$\begin{aligned} D_x(\mathbf{F}_{i,j}) &= \frac{1}{\Delta x} \left(\widehat{\mathbf{F}}_{i+\frac{1}{2},j} - \widehat{\mathbf{F}}_{i-\frac{1}{2},j} \right), & D_y(\mathbf{G}_{i,j}) &= \frac{1}{\Delta y} \left(\widehat{\mathbf{G}}_{i,j+\frac{1}{2}} - \widehat{\mathbf{G}}_{i,j-\frac{1}{2}} \right), \\ D_x(\mathbf{b}_{i,j}) &= \frac{1}{\Delta x} \left(\widehat{\mathbf{b}}_{i+\frac{1}{2},j} - \widehat{\mathbf{b}}_{i-\frac{1}{2},j} \right), & D_y(\mathbf{b}_{i,j}) &= \frac{1}{\Delta y} \left(\widehat{\mathbf{b}}_{i,j+\frac{1}{2}} - \widehat{\mathbf{b}}_{i,j-\frac{1}{2}} \right), \end{aligned}$$

The well-balanced compact finite difference scheme with TVB limiter for 2D problems (32) is given by:

$$\frac{\partial \mathbf{Q}}{\partial t} \Big|_{(x_i, y_j)} = -W_x^{-1} D_x(\mathbf{F}_{i,j}^{(m)}) + (\mathbf{A}^x)_{i,j} (\mathbf{B}_x)_{i,j} - W_y^{-1} D_y(\mathbf{G}_{i,j}^{(m)}) + (\mathbf{A}^y)_{i,j} (\mathbf{B}_y)_{i,j}, \quad (35)$$

where

$$\mathbf{b}_x = W_x^{-1} D_x(\mathbf{b}^{(m)}), \quad \mathbf{b}_y = W_y^{-1} D_y(\mathbf{b}^{(m)}).$$

The reconstructed numerical flux with TVB limiter as 1D case. To guarantee that scheme (35) is well-balanced, the limited reconstruction procedure for $\widehat{\mathbf{b}}_{i\pm\frac{1}{2},j}^{(m)}, \widehat{\mathbf{b}}_{i,j\pm\frac{1}{2}}^{(m)}$ have to be consistent with discharge term in $\widehat{\mathbf{F}}_{i\pm\frac{1}{2},j}^{(m)}, \widehat{\mathbf{G}}_{i,j\pm\frac{1}{2}}^{(m)}$, respectively, which is similar to the 1D well-balanced reconstruction.

We discuss the positivity and bound preserving of the first and the fourth equations in (35). We define the cell averages as $\bar{\mathbf{Q}} = W_x W_y \mathbf{Q}$. In particular, for h and $h\xi$, we have

$$\bar{h}_{ij}^{n+1} = \bar{h}_{ij}^n - \frac{\Delta t}{\Delta x} (W_y D_x (hu)^n)_{ij} - \frac{\Delta t}{\Delta y} (W_x D_y (hv)^n)_{ij}. \quad (36)$$

$$(\bar{h\xi})_{ij}^{n+1} = (\bar{h\xi})_{ij}^n - \frac{\Delta t}{\Delta x} (W_y D_x (h\xi u)^n)_{ij} - \frac{\Delta t}{\Delta y} (W_x D_y (h\xi v)^n)_{ij}. \quad (37)$$

Similar to the discussion in Section 3, under the CFL constraint

$$\frac{\Delta t}{\Delta x} \max |u| + \frac{\Delta t}{\Delta y} \max |v| \leq \frac{1}{3},$$

scheme (36) satisfies the weak monotonicity, i.e., \bar{h}_{ij}^{n+1} , $(\bar{h\xi})_{ij}^{n+1}$ are increasing function with respect to point values h_{ij}^n and $(h\xi)_{ij}^n$, respectively, which implies that if $h_{ij}^n \geq 0$, $m \leq (h\xi)_{ij}^n \leq M$, then $\bar{h}_{ij}^{n+1} \geq 0$, $m \leq (\bar{h\xi})_{ij}^{n+1} \leq M$.

When the TVB limiter is defined as above, weak monotonicity still holds under the CFL condition.

$$\frac{\Delta t}{\Delta x} \max |u| + \frac{\Delta t}{\Delta y} \max |v| \leq \frac{1}{12}. \quad (38)$$

If $\bar{h}_{ij}^{n+1} \geq 0$ and $m \leq (\bar{h\xi})_{ij}^{n+1} \leq M$, then the simple 3-point limiter in Algorithm 1 can be applied twice in a dimension-by-dimension fashion to post-process the point values for enforcing positivity and boundedness [17, 22].

Remark 3. *The CFL condition (38) is a sufficient condition for the forward Euler step to be weakly monotone, which is not a necessary condition to preserve bounds or positivity. When a third-order SSP Runge-Kutta method is used, the corresponding SSP stability coefficient is $c_s = \frac{1}{3}$, and a CFL like (31) is sufficient for the fully discrete scheme with SSP Runge-Kutta to preserve positivity and bounds.*

5 Numerical results for the Ripa Model

This section shows some numerical examples simulated by our proposed approach for 1D and 2D Ripa models. The gravitational constant is set as $g = 1$. The reference solutions are computed as the fine mesh with 2000 grid points in most cases. All testing cases except the accuracy and well-balanced tests adopt the inflow and outflow boundary conditions. We set $\text{CFL} = \frac{1}{12}$ for efficiency as mentioned in Remark 3.

5.1 One-dimensional test problems

5.1.1 Well-balanced property

This test is used to verify the well-balanced property of the proposed compact finite difference scheme. The initial conditions are set with a steady state $h + b = 10$, $u = 0$ and $\theta = 0.1$, with smooth and discontinuous bottom topographies,

$$b(x) = 5 \exp\left(-\frac{2}{5}(x-5)^2\right), \quad \text{and} \quad b(x) = \begin{cases} 4.0, & 4 \leq x \leq 8, \\ 0.0, & \text{otherwise.} \end{cases} \quad (39)$$

The problem is computed on $x \in [0, 10]$ up to $t = 0.5$ using exact boundary conditions. The minmod parameter γ is taken as 0.02. The L^1 errors of h , hu and $h\theta$ are shown in Table 1. We observe that round-off errors are reached for both bottom topographies, confirming the expected well-balanced property.

Table 1: C-property test. The L^1 errors of $h + b$, hu , and $h\theta$ with different bottom topographies.

N	Smooth bottom topography			Discontinuous bottom topography		
	$h + b$	hu	$h\theta$	$h + b$	hu	$h\theta$
50	2.41E-16	1.10E-15	1.06E-16	2.04E-16	2.47E-16	2.08E-17
100	1.77E-15	1.39E-15	1.22E-16	4.35E-16	3.64E-16	3.63E-17
200	2.02E-15	1.56E-15	2.89E-16	5.74E-16	6.28E-16	8.92E-17
400	2.56E-15	1.72E-15	2.89E-16	9.15E-16	6.50E-16	1.05E-16

5.1.2 Accuracy test

This test is taken from [21], used to check the numerical order of accuracy of the proposed scheme for a smooth solution. The bottom topography is given by $b(x) = 0.1 \sin(4\pi x) - 1$. The initial conditions are

$$(h, hu, \theta)(x, 0) = (1.0 - b(x), 0.1, 1.0 + 0.01 \cos(2\pi(x - 0.5))).$$

The computational domain is $x \in [0, 1]$ with periodic boundary conditions. The final time is $t = 1$. The minmod parameter is taken as $\gamma = 10000$ for the smooth problems. To test the fourth-order spatial accuracy, we set the time step as $\Delta t = (\text{CFL}\Delta x/\alpha)^{4/3}$, where $\alpha = \max_{x \in [0, 1]} |\lambda|$ with λ being the max eigenvalues of the Jacobian matrix $\partial \mathbf{F}(\mathbf{Q})/\partial \mathbf{Q}$. The reference solution computed by the proposed scheme with $N = 6400$ is treated as the exact solution to calculate the leading errors. The L^1 errors of h , hu and $h\theta$ are shown in Table 2. It is clearly seen that the optimal fourth-order accuracy is achieved.

Table 2: L^1 errors and convergence orders for the test case in Section 5.1.2.

N	h		hu		$h\theta$	
	L^1 -error	Order	L^1 -error	Order	L^1 -error	Order
25	3.68E-07		7.00E-07		3.66E-07	
50	2.13E-08	4.11	4.18E-08	4.07	2.12E-08	4.11
100	1.31E-09	4.02	2.58E-09	4.01	1.31E-09	4.02
200	8.17E-11	4.01	1.61E-10	4.00	8.14E-11	4.01
400	5.10E-12	4.00	1.01E-11	4.00	5.09E-12	4.00
800	2.91E-13	4.13	5.63E-13	4.16	2.88E-13	4.14

5.1.3 Riemann problem over a flat bottom

This test from [5] consists of rarefaction, contact wave, and shock. We test this example to check the shock-capturing properties of the considered numerical algorithm. The flat bottom topography ($b(x) \equiv 0$) is used. The initial conditions with a discontinuous constant on $x \in [-1, 1]$ is given by

$$(h, u, \theta)(x, 0) = \begin{cases} (5.0, 0.0, 3.0), & x < 0, \\ (1.0, 0.0, 5.0), & x \geq 0. \end{cases}$$

We perform the numerical test up to $t = 0.2$ with $N = 200$ as illustrated in Figure 1. The minmod parameter is taken as $\gamma = 0.02$. In this test, we utilize the bound-preserving limiter in Algorithm 1 to enforce the lower and upper bound of θ . There are no spurious pressure oscillations in the neighborhood of temperature jumps. The jumps around the contact wave located near $x = 0.43$ are sharply resolved. This test effectively demonstrates the shock-resolution properties and the effectiveness of the bound-preserving limiter for θ .

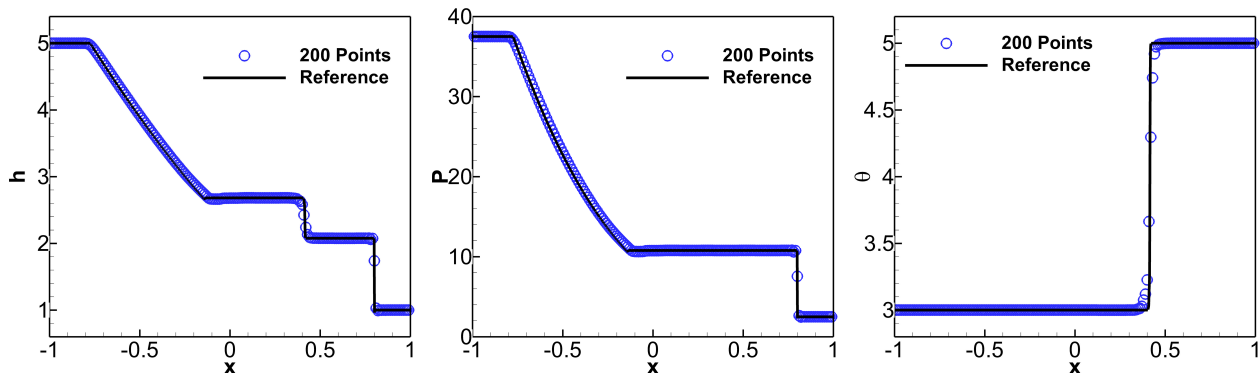


Figure 1: The numerical solutions of depth h , pressure P and temperature θ in Riemann problem over a flat bottom in Section 5.1.3.

We take this test to exhibit how sensitive are the numerical results to the choice of parameter γ . We show depth h , pressure P and temperature θ with $\gamma = 0, 100$ in Figure 2. No significant differences are observed among the various parameter choices in this test. We also test $\gamma = 0.2, 2, 10$ with the same conclusion that the parameter γ is non-sensitive in this test.

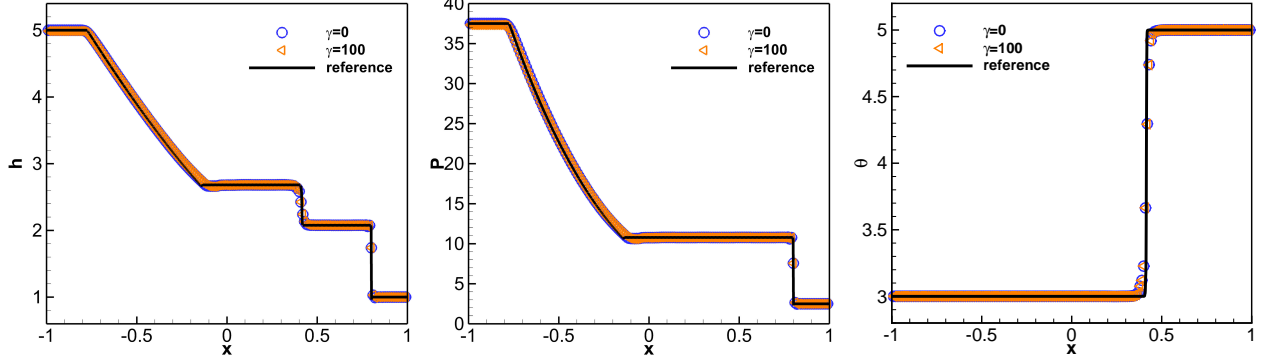


Figure 2: The numerical solutions of depth h , pressure P and temperature θ in Riemann problem over a flat bottom with different γ in Section 5.1.3.

5.1.4 Dam break problem over a flat bottom

We consider the dam break problem in [5] over a flat bottom ($b(x) \equiv 0$) with the initial conditions

$$(h, u, \theta)(x, 0) = \begin{cases} (2.0, 0.0, 1.0), & |x| \leq 0.5, \\ (1.0, 0.0, 1.5), & |x| > 0.5. \end{cases} \quad (40)$$

The problem is computed on $x \in [-1, 1]$. The minmod parameter γ is taken as 0.02. The results are illustrated in Figure 3 with a spatial resolution of $N = 200$ up to $t = 0.2$. One can observe that our scheme maintains the bounds of θ and performs well in capturing the shocks and contact discontinuities without numerical oscillations.

We use this test to illustrate the influence of different choices of γ . We show depth h , pressure P and temperature θ with $\gamma = 0, 100$ in Figure 4. One can see that there are obvious oscillations when $\gamma = 100$. We also test $\gamma = 0.2, 2, 10$ and found that they look similar to $\gamma = 0$, meaning that once γ exceed a certain threshold, the TVB limiter would decrease the property of removing oscillations.

5.2 Two-dimensional problems

5.2.1 Two-dimensional accuracy test

In this test, we verify the numerical orders of accuracy when the proposed schemes are applied to a two-dimensional case. The bottom topography and the initial conditions are given by

$$b(x, y) = \sin(2\pi x) + \cos(2\pi y), \quad (h, hu, hv, h\theta) = \begin{cases} 10 + e^{\sin(2\pi x)} \cos(2\pi y), \\ \sin(\cos(2\pi x)) \sin(2\pi y), \\ \cos(2\pi x) \cos(\sin(2\pi y)), \\ 0.5e^{-100(x-0.5)^2 - 100(y-0.5)^2}. \end{cases}$$

The minmod parameter is taken as $\gamma = 10000$ for the smooth problems. The time step setting is the same as that in 1D case. The final time is taken as $t = 0.015$, maintaining smooth solutions.

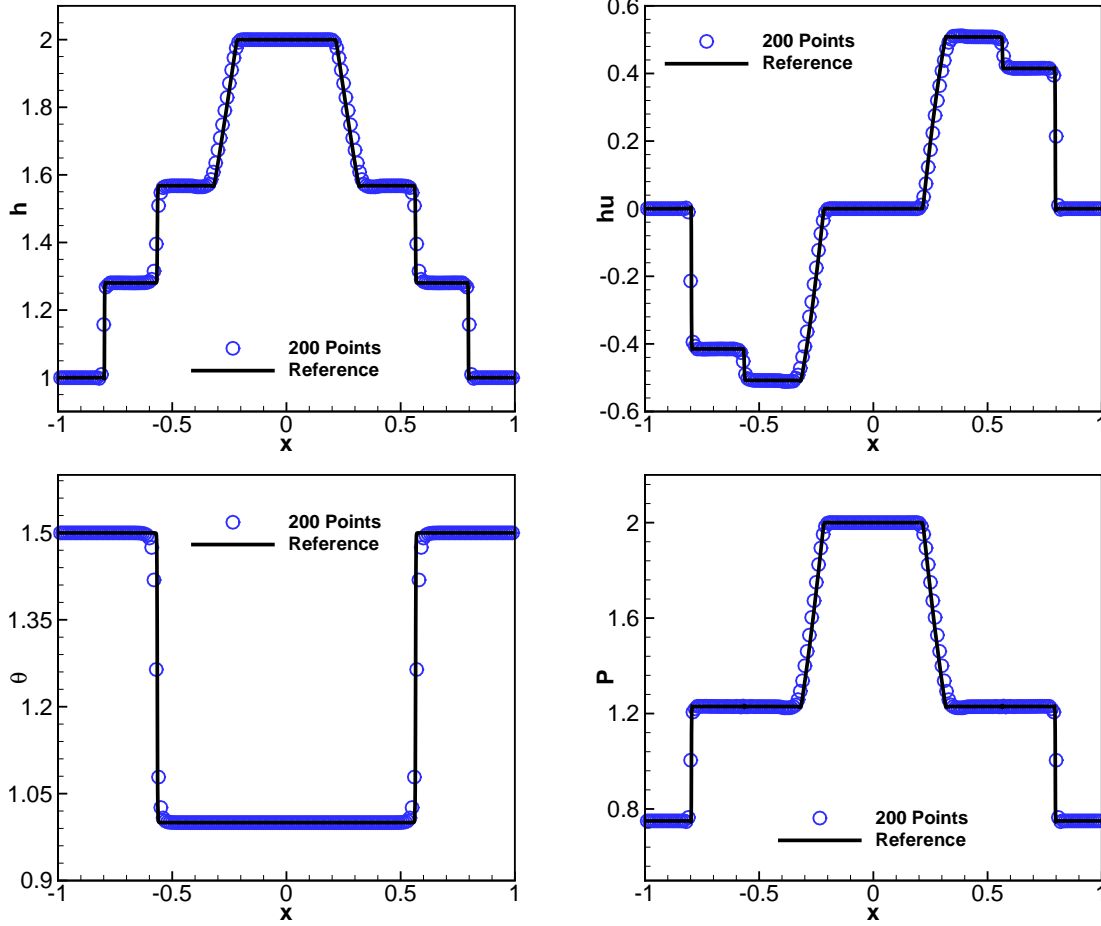


Figure 3: Distributions of the height h , momentum hu , temperature θ , and pressure p of the dam break problem over a flat bottom in Section 5.1.4.

Since the analytic solution of this problem is explicitly unknown, we treat the proposed scheme with 800×800 mesh as a reference solution. Table 3 contains the L^1 errors and convergence orders of the proposed scheme. One can see that the optimal fourth-order accuracy is achieved.

Table 3: L^1 errors and convergence orders for the test case in Section 5.2.1.

$N_x \times N_y$	h		hu		hv		$h\theta$	
	L^1 -error	Order						
25×25	5.05E-05		7.15E-05		5.45E-05		7.65E-06	
50×50	2.78E-06	4.18	8.20E-06	3.12	3.27E-06	4.06	4.12E-07	4.22
100×100	1.75E-07	3.99	7.24E-07	3.50	2.18E-07	3.91	2.56E-08	4.01

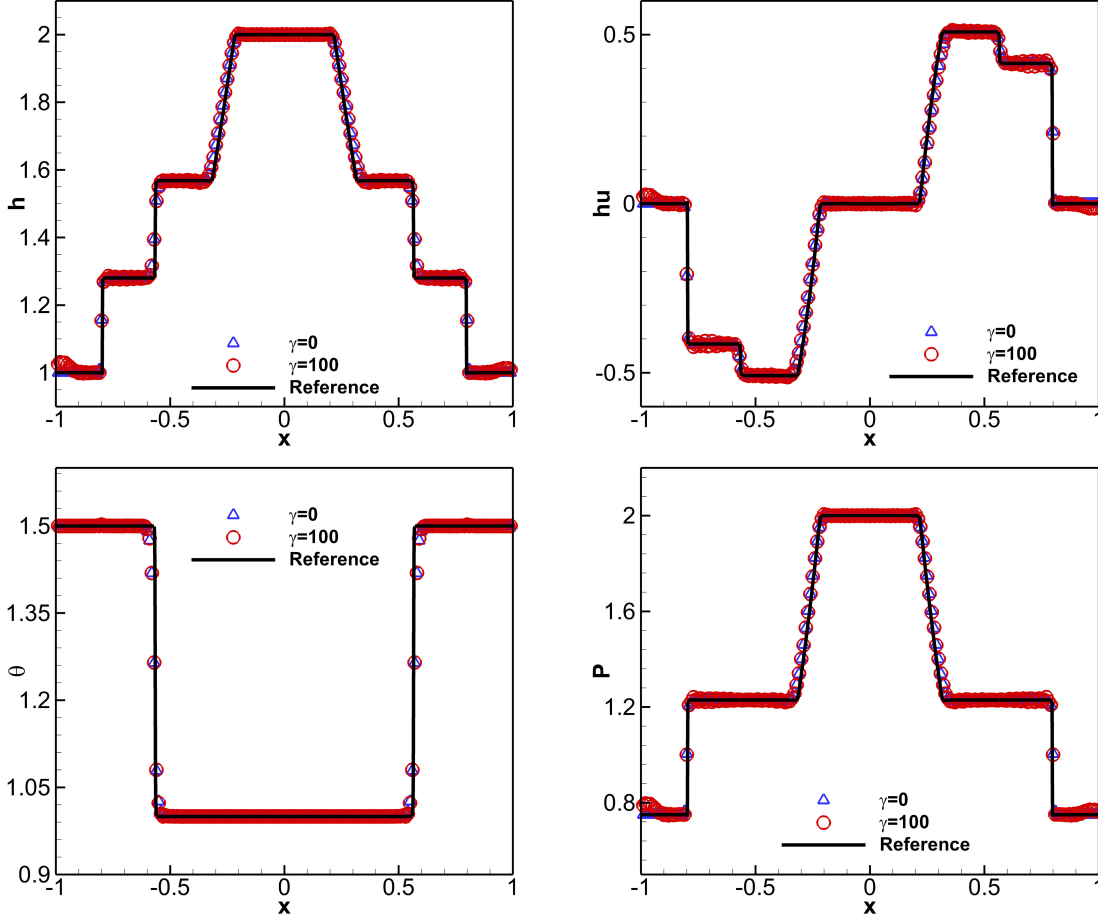


Figure 4: Distributions of the height h , momentum hu , temperature θ , and pressure p with different γ of the dam break problem over a flat bottom in Section 5.1.4.

5.2.2 Small perturbation of the steady state solution

The goal of this example is to check the well-balanced property and capability of capturing small amplitude perturbation of steady state in two-dimension with two Gaussian-shaped humps bottom.

$$b(x, y) = \begin{cases} 0.5 \exp(-100((x + 0.5)^2 + (y + 0.5)^2)), & x < 0, \\ 0.6 \exp(-100((x - 0.5)^2 + (y - 0.5)^2)), & x \geq 0. \end{cases}$$

The initial condition for small perturbation of a steady state is given by:

$$(h, u, v, \theta)(x, y, 0) = \begin{cases} (3.1 - b(x, y), 0.0, 0.0, \frac{4}{3}), & 0.1 \leq r < 0.3, \\ (3.0 - b(x, y), 0.0, 0.0, \frac{4}{3}), & 0.3 \leq r < 0.5, \text{ or } r < 0.1, \\ (2.0 - b(x, y), 0.0, 0.0, 3.0), & r \geq 0.5, \end{cases}$$

where $r = \sqrt{x^2 + y^2}$. We simulate the small perturbation test up to $t = 0.15$. Exact boundary conditions are employed. The minmod parameter γ is taken as 0.3. 3D plots of the surface $h + b$, temperature θ and pressure P computed in $(x, y) \in [-1, 1] \times [-1, 1]$ with 200×200 cells are shown in Figure 5. The contour levels for $h + b, \theta, P$ are shown in Figure 6. The proposed scheme accurately captured the physical structures of small perturbations of steady state, which verifies the well-balanced property of the proposed compact finite difference scheme.

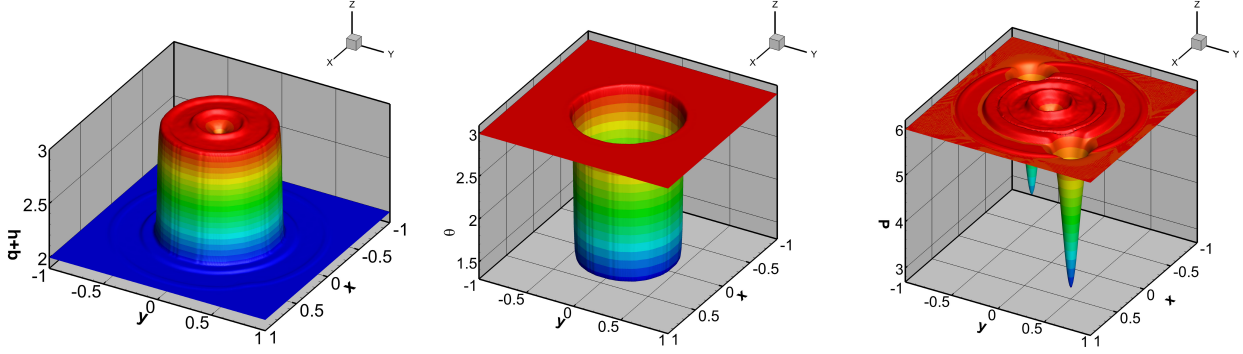


Figure 5: 3D plots of the small perturbation problems at time $t = 0.15$ in Section 5.2.2.

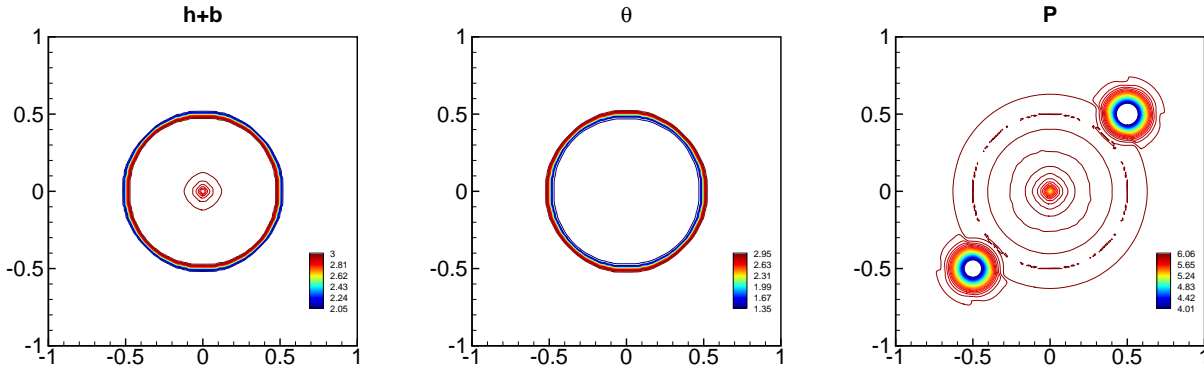


Figure 6: Contour levels with 30 lines of the small perturbation problems at time $t = 0.15$ in Section 5.2.2.

5.2.3 Dam break problem over a flat bottom

We consider a dam break problem in [1] with flat bottom ($b(x, y) = 0$) in the computational domain $[-1, 1] \times [-1, 1]$. Initially, the thin dam is described by:

$$(h, u, v, \theta)(x, y, 0) = \begin{cases} (2.0, 0.0, 0.0, 1.0), & r < 0.5, \\ (1.0, 0.0, 0.0, 1.5), & r \geq 0.5. \end{cases}$$

The dam is located at $r = 0.5$, where $r = \sqrt{x^2 + y^2}$. When the dam collapses, there are different depths and temperatures inside and outside. The minmod parameter γ is taken as 0.3. 3D plots of the water depth h , temperature θ , and pressure P are displayed in Figure 7 at the final time $t = 0.15$ with 200×200 cells. We use the bound-preserving limiter for water depth and temperature. One can observe that the proposed scheme captured the discontinuities of the solutions without unphysical oscillations.

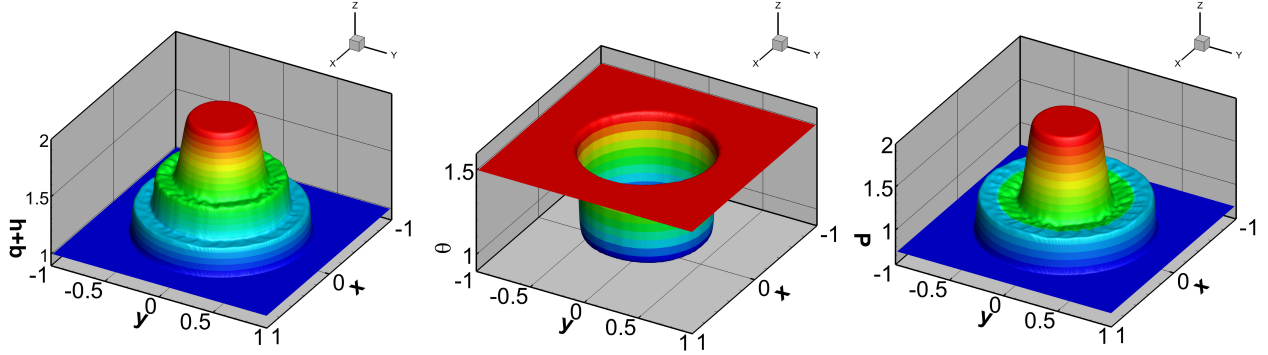


Figure 7: 3D plots of the water depth h , temperature θ and pressure p of the dam break problem studied in Section 5.2.3 using 200×200 cells.

6 Numerical results for pollutant transport model

This section presents pollutant transport simulations in one and two dimensions. The gravitational constant is set as $g = 9.812$. The setting about boundary conditions and CFL conditions are the same as those in Section 5.

6.1 One-dimensional test problems

The well-balanced properties and accuracy of the 1D pollutant transport model have also been checked with a similar conclusion to those of the Ripa model. We omit the results to save space and only show the representative results.

6.1.1 Advection of pollutant over variable bottom topography

In this test, we will numerically track pollutant propagation over the variable bottom [8]. The initial water level is constant, and the pollutant moves from left to right. The initial setup is

$$(h, hu, T)(x, 0) = \begin{cases} (1 - b(x), 0.1, 1.0), & 0.4 \leq x \leq 0.5, \\ (1 - b(x), 0.1, 0.0), & \text{otherwise,} \end{cases}$$

where the bottom topography is set as

$$b(x) = \begin{cases} 0.25(\cos(10\pi(x - 1.5)) + 1), & 0.4 \leq x \leq 0.6, \\ 0.0, & \text{otherwise.} \end{cases}$$

The pollutant concentration is tracked at times $t = 0, 2, 4$ within computational domain $x \in [0, 1]$. The minmod parameter γ is taken as 10^{-5} . The numerical evolution is shown in Figure 8 with 200 points and compared with the reference solution with 2000 points. One can find that the concentration is bounded during the whole time evolution. Our numerical results have less diffusion than those in [20] as well as the Central scheme.

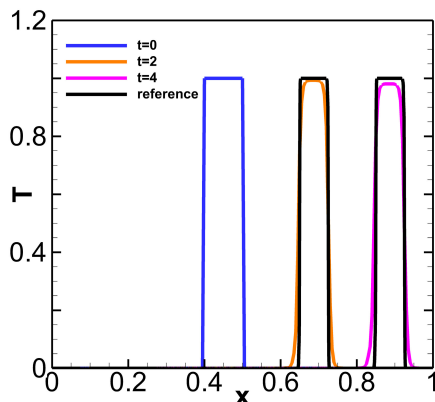


Figure 8: Pollutant concentration T at times $t = 0, 2, 4$ in advection of pollutant in Section 6.1.1.

6.1.2 Small perturbation imposed to a steady state water body

There is a small perturbation imposed locally on the steady-state solutions. The initial conditions are given by:

$$(h, u, T)(x, 0) = \begin{cases} (1.2 - b(x), 0.0, 0.1), & 1.1 \leq x \leq 1.2, \\ (1.0 - b(x), 0.0, 0.1), & \text{otherwise,} \end{cases}$$

where the bottom topography is set as

$$b(x) = \begin{cases} 0.25(\cos(10\pi(x - 1.5)) + 1), & 1.4 \leq x \leq 1.6, \\ 0.0, & \text{otherwise.} \end{cases}$$

The problem is simulated with 200 grids in the computational domain $x \in [0, 2]$ up to $t = 0.2$. The minmod parameter γ is taken as 10^{-5} . The numerical results are shown in Figure 9. It can be clearly observed that the numerical solutions agree well with the reference ones. The numerical results accurately resolve small perturbations of a steady-state solution, which verified the well-balanced property of the proposed scheme.

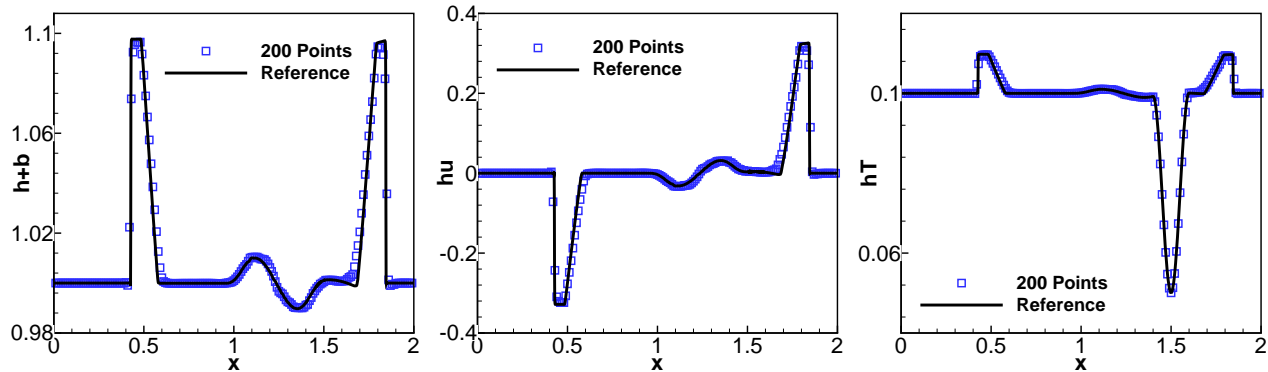


Figure 9: Numerical surface $h + b$, momentum hu and quantity of pollutant hT with $N = 200$ for small perturbation problem in Section 6.1.2. The final time is $t = 0.2$.

6.2 2D numerical results

6.2.1 Circular dam break

This test example is similar to the dam break problem in the Ripa model in Section 5.2.3. Initially, there is an infinitely thin circular dam. Upon instantaneous collapse of the dam, the flow becomes transcritical. The radius of dam is $r = \sqrt{x^2 + y^2} = 2.5$ in $(x, y) \in [-20, 20] \times [-20, 20]$. The initial conditions are given by:

$$(h, u, v, T)(x, y, 0) = \begin{cases} (2.5, 0.0, 0.0, 1.0), & r \leq 2.5, \\ (0.5, 0.0, 0.0, 0.5), & r > 2.5. \end{cases} \quad (41)$$

The problem is computed with 300×300 cells up to $t = 0.45$. The minmod parameter γ is taken as 0.3. Numerical results for water depth h , pollutant concentration T , and hT are presented in Figure 10. We observe that smoothly preserves the maximum and minimum value of the pollutant concentration. The water height shock front is well captured. The results agree well with those in [16]. This example demonstrates the effectiveness of the proposed scheme and bound-preserving limiter.

6.2.2 Dam break with scalar transport

The goal of this set of numerical experiments from [12] is to verify the performance of the positivity-preserving and bound-preserving properties of the proposed scheme. The dam is located at $x_0 = 10$ with different downstream water depths.

The initial conditions are given by

$$(h, u, v, T)(x, y, 0) = \begin{cases} (1.0, 0.0, 0.0, 1.0), & x \leq 10, \\ (h_0, 0.0, 0.0, 1.0), & x > 10, \end{cases}$$

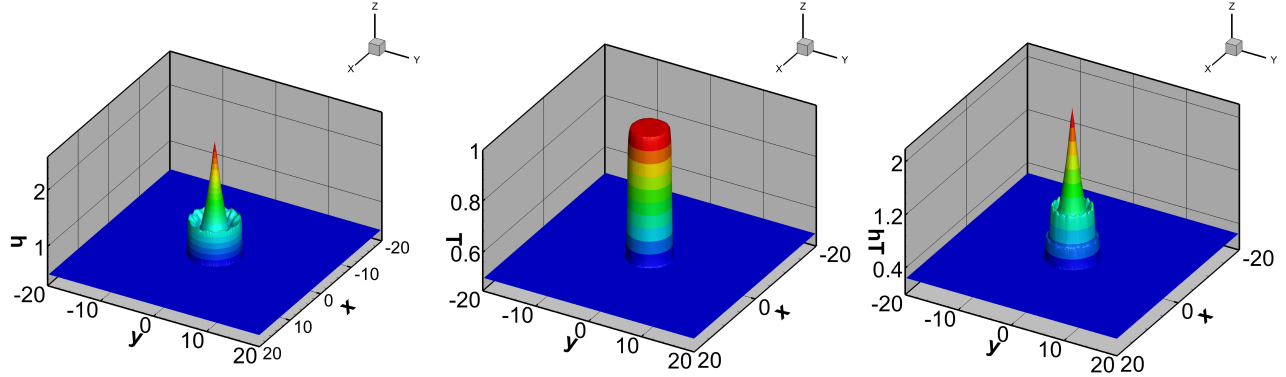


Figure 10: Numerical water depth h , concentration of pollutant T and quantity of pollutant hT for a circular dam break in Section 6.2.1 at time $t = 0.45$.

on a computational domain $[0, 20] \times [-5, 5]$ where $h_0 = 0.1$ is set for the wet case and $h_0 = 0$ is used for the dry case. The minmod parameter γ is taken as 10^{-5} . We implement the bound-preserving limiter for water depth and polluted concentration. We adopt the same numerical treatment as in [12, 13] to avoid dividing by zero water depth. Numerical results for water depth h and $1 - T$ in two cases are presented in Figure 11 with uniformed 200×100 cells at $t = 1$. We compare the results of the proposed numerical method with the one-dimensional analytical solutions in [7]. The non-negative water height verifies the effectiveness of the positivity-preserving limiter, and the bounded pollutant concentration verifies the effectiveness of the bound-preserving limiter.

6.2.3 Passive scalar advection

In this numerical example, we consider the advection of pollutant by shallow water flows over flat bed to verify the bound-preserving property of the proposed scheme. The water depth is initially constant with $h = 1.0$, the velocity of the flow is $u = v = 0.5$, and the initial pollutant concentration is given by:

$$T(x, y, 0) = \begin{cases} 1, & (x - 1.5)^2 + (y - 1.5)^2 \leq 1, \\ 0, & \text{otherwise.} \end{cases} \quad (42)$$

We compute in $[0, 10] \times [0, 10]$ using 250×250 cells. The minmod parameter γ is taken as 0.3. The concentration results up to $t = [1, 4, 8, 12]$ are presented in Figure 12. The minimum and maximum concentration during the $t \in (0, 12)$ are presented in Figure 13. One can observe the concentration is accurately approximated and bounded with free-oscillation, the constant state of the concentration is preserved in the whole domain. The shape and movement of flows are comparable to the results with those in [12]. The test can demonstrate that our proposed scheme performs well for diffusion process.

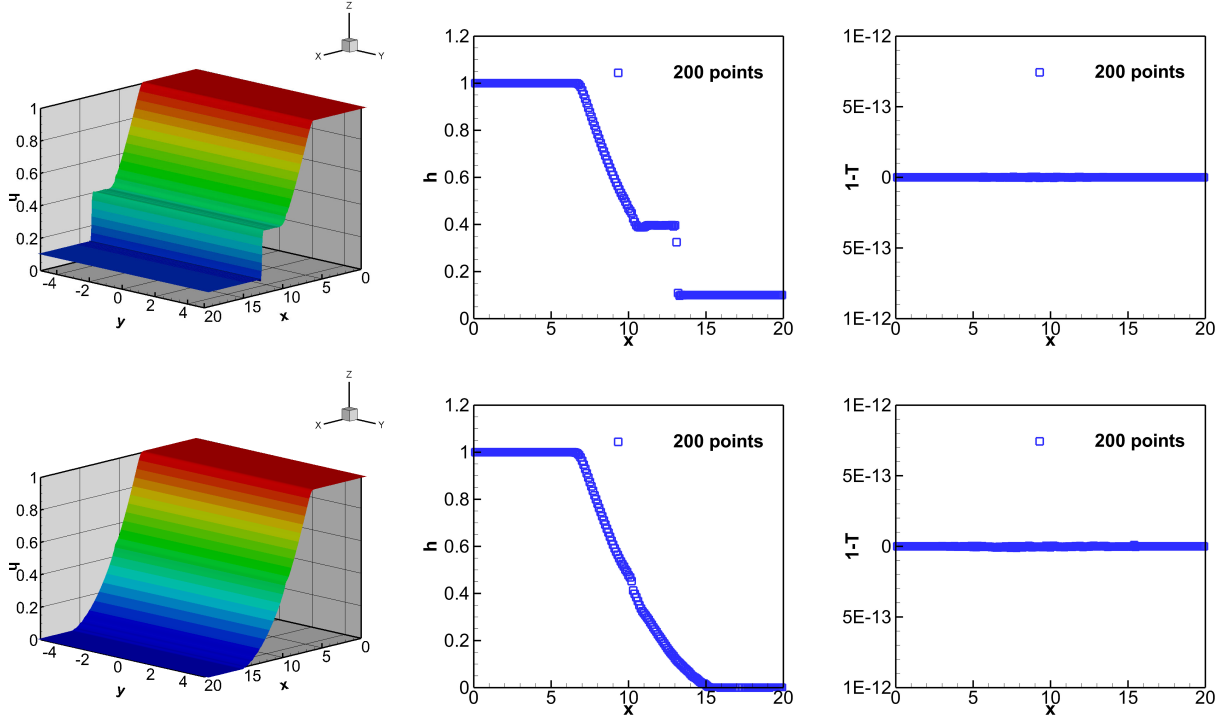


Figure 11: Dam break with scalar pollutant transport results in Section 6.2.2. Wet case (top line) and dry case (bottom line) at time $t = 1$.

6.2.4 Dam break on a non-flat bottom with nonzero source

We consider the two-dimensional dam-break problem [4] involving the release of a polluted source on the domain $[-300, 1100] \times [0, 1400]$ with a non-flat bottom topography. The initial dam setting is shown on the left of Figure 14. The shape of the dam is given by

$$\Gamma(y) = 200 + \begin{cases} \min \left\{ \frac{(y-700)^2}{400}, 400 \right\}, & y < 700, \\ 0, & y \geq 700. \end{cases}$$

The bottom topography consists of three elliptically-shaped exponential humps, given by:

$$b(x, y) = 4.5 \cdot \sum_{k=1}^3 \exp(-E_k(x, y)), \quad E_k(x, y) = \frac{(x - x_k)^2}{a_k} + \frac{(y - y_k)^2}{b_k},$$

with

$$(x_k, y_k, a_k, b_k) = \begin{cases} (500, 700, 10^4, 10^3), & k = 1, \\ (300, 600, 10^3, 10^4), & k = 2, \\ (700, 700, 10^3, 10^4), & k = 3. \end{cases}$$

The initially curved shock wave interacting with a complicated nonflat bottom will result in complicated structures. Beginning with clean water, a time-dependent pollutant source $S(x, y, t)$ is

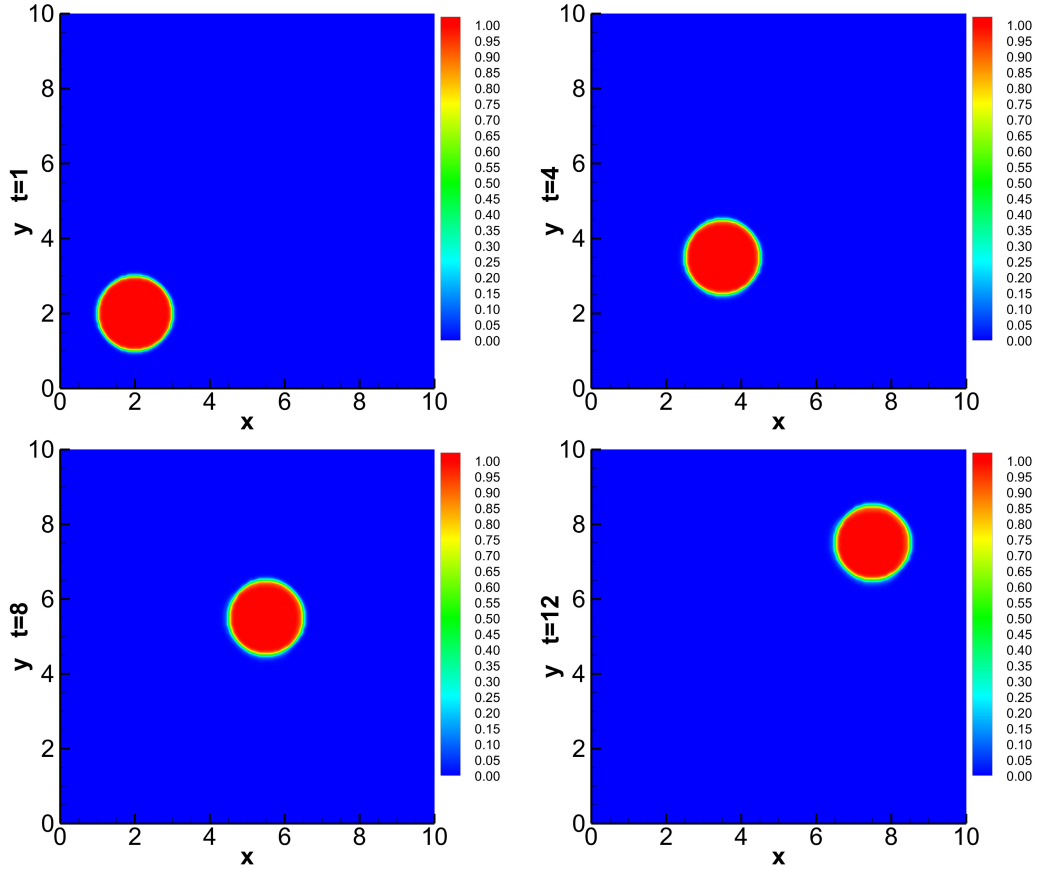


Figure 12: Passive scalar advection results are presented in Section 6.2.3. From left-to-right and top-to-bottom: Concentration results are shown at time $t = 1, 4, 8$ and 12 .

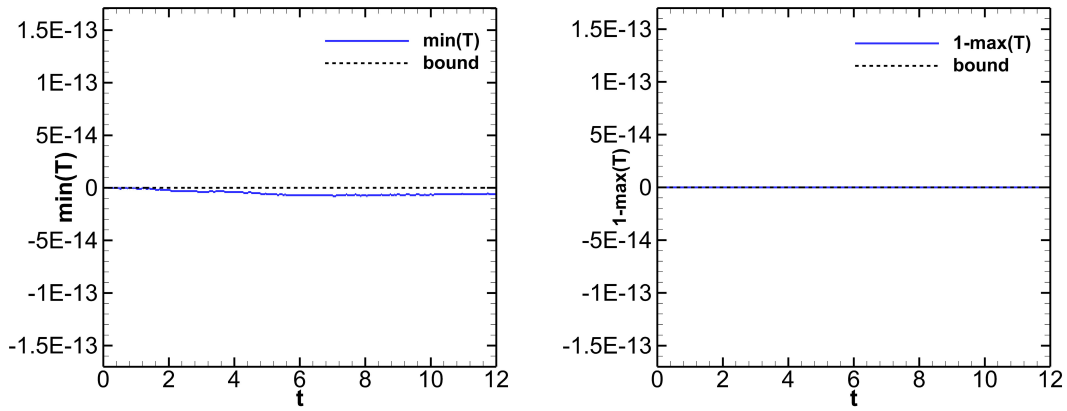


Figure 13: Concentration results in passive scalar advection in Section 6.2.3. Left: $\min(T)$ and Right: $1 - \max(T)$.

released. The effect of pollutant source can be incorporated into the right-hand side of the fourth equation of (32), which is modeled by the transport equation,

$$(hT)_t + (hTu)_x + (hTv)_y = T_S S,$$

where pollutant concentration of $T_S = 25$ is released together with

$$S(x, y, t) = 0.5 \exp \left(-0.5(t - 8)^2 - 0.00001(x + y - 1000)^2 - 0.0005(x - y + 200)^2 \right).$$

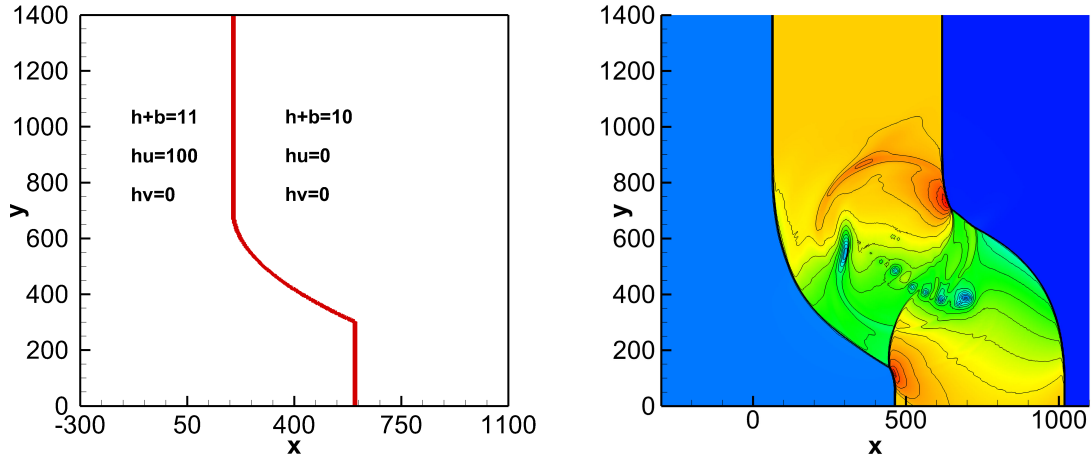


Figure 14: Initial setting in Example 6.2.4 (left) and contour plot of $h + b$ at $t = 30$ (right).

The problem is computed with 500×500 cells up to $t = 30$. The minmod parameter γ is taken as 10^{-5} . We can see from the right part of Figure 14 that the proposed scheme can capture complicated structures while initially curved shock waves interact with a complicated nonflat bottom. The proposed compact finite difference scheme has a good resolution for capturing complex small-scale structures inside the vortices. The time evolution of the h and T is tracked in Figure 15, and Figure 16, respectively. The numerical results well capture the advection-difusion processes of pollutant transport with the influence of source contaminants. The depicted numerical structures and results with time evolutions compare favorably with that presented in [4, 16].

7 Concluding remarks

We have constructed a fourth-order well-balanced compact finite difference scheme, which preserves positivity and bounds for the Ripa and pollutant transport equations in a unified framework. To ensure nonlinear stability, we use a TVB limiter to reconstruct stable numerical fluxes, for which the well-balanced property is achieved by properly approximating the source term with the TVB limiter incorporated. The weak monotonicity in the compact finite difference scheme is leveraged to establish and ensure the positivity and bound-preserving properties. Notably, positivity and

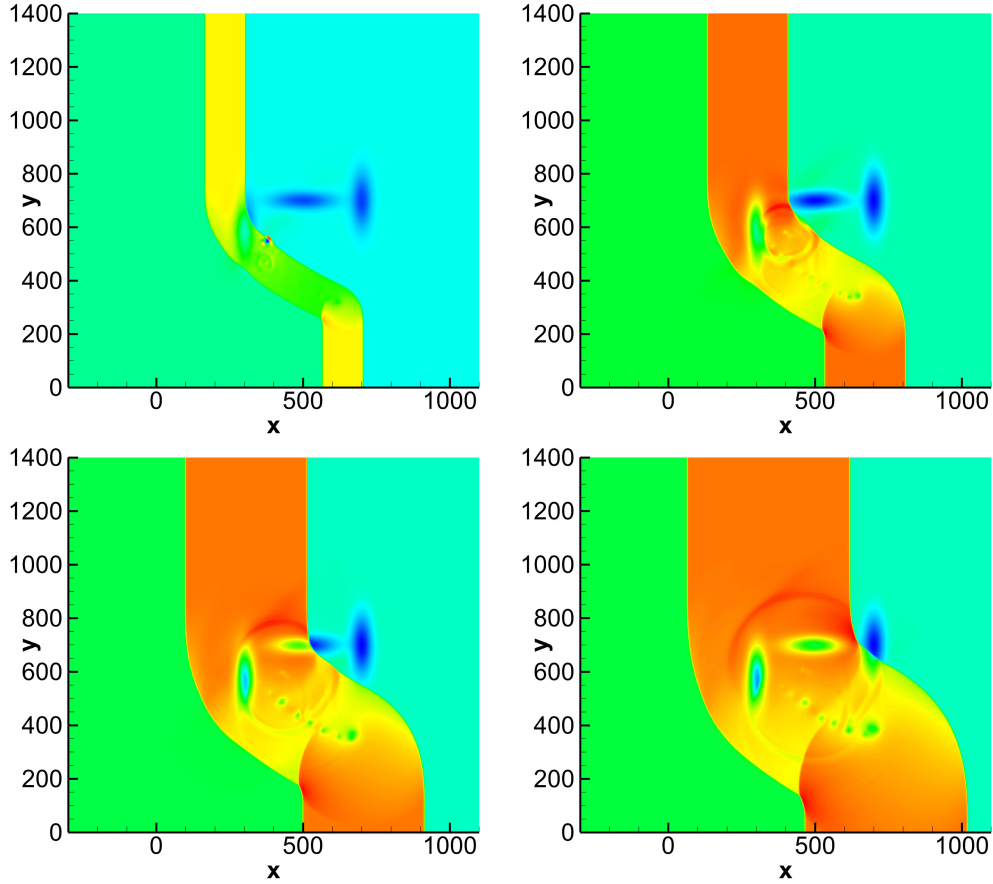


Figure 15: Top view on h evolution in Section 6.2.4 at times $t = 7.5, 15, 22.5, 30$ (from top to down and from left to right).

bounds can be enforced by the same simple limiter without compromising the well-balanced nature and conservation of the scheme. Extensive numerical tests demonstrate the robustness, high-order accuracy, positivity, and bound preservation capabilities of the proposed method.

Acknowledgement

The work of Ren, Wang, and Gao is supported by the National Natural Science Foundation of China (No. 12371435), Shandong Provincial Natural Science Foundation (No. ZR2023MA043), and Tais-han Scholars Program (tsqn202211059). The work of Ren is also supported by the China Scholarship Council fellowship. The work of Wang is supported by the National Natural Science Foundation of China (No. 12301530), Shandong Provincial Natural Science Foundation (No. ZR2022MA012), and Shandong Provincial Qingchuang Science and Technology Project (No. 2023KJI020). The work of Zhang is supported by NSF DMS-1913120. The author (Wang) also thanks Hong Kong Baptist University for providing a conducive environment for conducting this research during his visits.

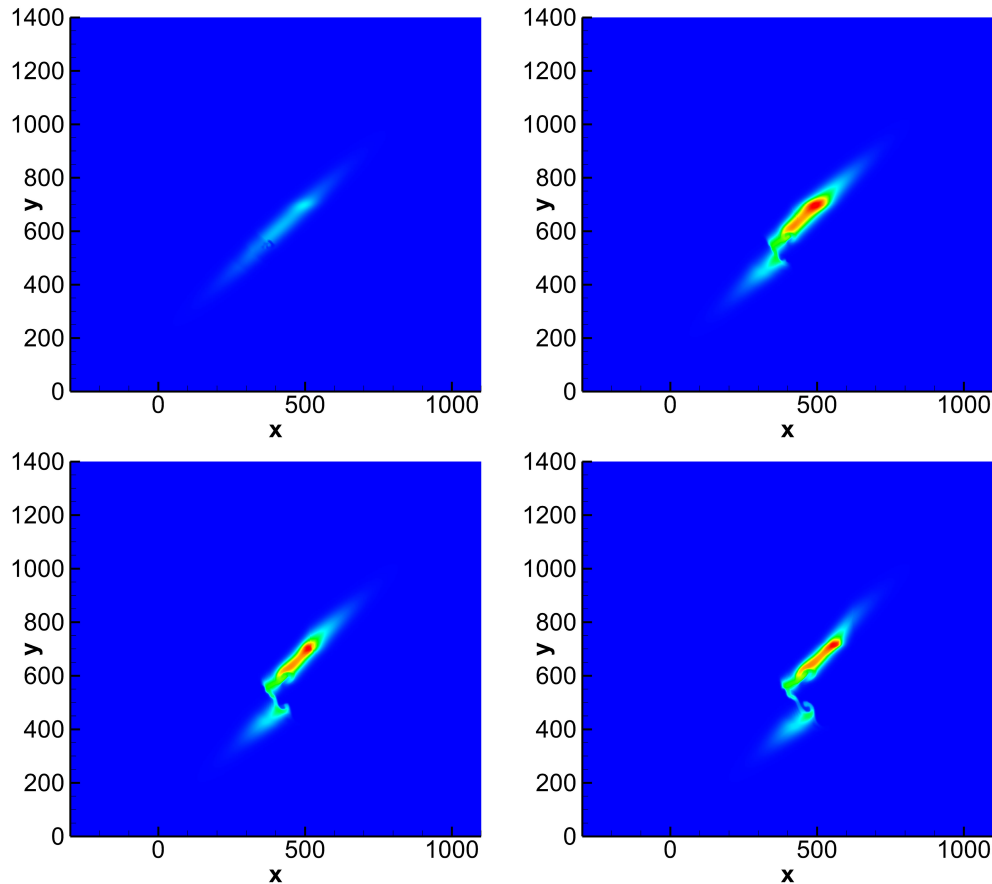


Figure 16: Top view on T evolution in Section 6.2.4 at times $t = 7.5, 15, 22.5, 30$ (from top to down and from left to right).

References

- [1] M. BAER AND J. NUNZIATO, *A two-phase mixture theory for the deflagration-to-detonation transition (ddt) in reactive granular materials*, International Journal of Multiphase Flow, 12 (1986), pp. 861–889.
- [2] A. BERMUDEZ AND M. E. VAZQUEZ, *Upwind methods for hyperbolic conservation laws with source terms*, Computers & Fluids, 23 (1994), pp. 1049–1071.
- [3] J. BRITTON AND Y. XING, *High order still-water and moving-water equilibria preserving discontinuous Galerkin methods for the Ripa model*, Journal of Scientific Computing, 82 (2020), pp. 1–37.
- [4] A. CHERTOCK AND A. KURGANOV, *On a hybrid finite-volume-particle method*, ESAIM: Mathematical Modelling and Numerical Analysis, 38 (2004), pp. 1071–1091.

- [5] A. CHERTOCK, A. KURGANOV, AND Y. LIU, *Central-upwind schemes for the system of shallow water equations with horizontal temperature gradients*, *Numerische Mathematik*, 127 (2014), pp. 595–639.
- [6] B. COCKBURN AND C.-W. SHU, *Nonlinearly stable compact schemes for shock calculations*, *SIAM Journal on Numerical Analysis*, 31 (1994), pp. 607–627.
- [7] O. DELESTRE, C. LUCAS, P.-A. KSINANT, F. DARBOUX, C. LAGUERRE, T.-N.-T. VO, F. JAMES, AND S. CORDIER, *Swashes: a compilation of shallow water analytic solutions for hydraulic and environmental studies*, *International Journal for Numerical Methods in Fluids*, 72 (2013), pp. 269–300.
- [8] A. DELIS AND T. KATSAOUNIS, *A generalized relaxation method for transport and diffusion of pollutant models in shallow water*, *Computational Methods in Applied Mathematics*, 4 (2004), pp. 410–430.
- [9] V. DESVEAUX, M. ZENK, C. BERTHON, AND C. KLINGENBERG, *Well-balanced schemes to capture non-explicit steady states: Ripa model*, *Mathematics of Computation*, 85 (2016), pp. 1571–1602.
- [10] J. DONG AND X. QIAN, *Well-balanced and positivity-preserving surface reconstruction schemes solving Ripa systems with nonflat bottom topography*, *SIAM Journal on Scientific Computing*, 44 (2022), pp. A3098–A3129.
- [11] W. HUANG, R. LI, J. QIU, AND M. ZHANG, *A well-balanced moving mesh discontinuous Galerkin method for the Ripa model on triangular meshes*, *Journal of Computational Physics*, 487 (2023), p. 112147.
- [12] H. KARJOUN, A. BELJADID, AND P. G. LEFLOCH, *A well-balanced positivity preserving cell-vertex finite volume method satisfying the discrete maximum-minimum principle for coupled models of surface water flow and scalar transport*, arXiv preprint arXiv, 2012.13702 (2020).
- [13] A. KURGANOV AND G. PETROVA, *A second-order well-balanced positivity preserving central-upwind scheme for the Saint-Venant system*, *Communications in Mathematical Sciences*, 5 (2007), pp. 133–160.
- [14] M. E. LEE AND I. W. SEO, *2D finite element pollutant transport model for accidental mass release in rivers*, *KSCE Journal of Civil Engineering*, 14 (2010), pp. 77–86.
- [15] S. K. LELE, *Compact finite difference schemes with spectral-like resolution*, *Journal of Computational Physics*, 103 (1992), pp. 16–42.
- [16] G. LI, J. GAO, AND Q. LIANG, *A well-balanced weighted essentially non-oscillatory scheme for pollutant transport in shallow water*, *International Journal for Numerical Methods in Fluids*, 71 (2013), pp. 1566–1587.

- [17] H. LI, S. XIE, AND X. ZHANG, *A high order accurate bound-preserving compact finite difference scheme for scalar convection diffusion equations*, SIAM Journal on Numerical Analysis, 56 (2018), pp. 3308–3345.
- [18] W. MERRITT, R. LETCHER, AND A. JAKEMAN, *A review of erosion and sediment transport models*, Environmental Modelling & Software, 18 (2003), pp. 761–799.
- [19] L. MONTHE, F. BENKHALDOUN, AND I. ELMAHI, *Positivity preserving finite volume Roe: schemes for transport-diffusion equations*, Computer Methods in Applied Mechanics and Engineering, 178 (1999), pp. 215–232.
- [20] O. RABBANI, M. AHMED, AND S. ZIA, *Transport of pollutant in shallow flows: A space-time CE/SE scheme*, Computers & Mathematics with Applications, 77 (2019), pp. 3195–3211.
- [21] A. REHMAN, I. ALI, S. ZIA, AND S. QAMAR, *Well-balanced finite volume multi-resolution schemes for solving the Ripa models*, Advances in Mechanical Engineering, 13 (2021), pp. 1–16.
- [22] B. REN, Z. GAO, Y. GU, S. XIE, AND X. ZHANG, *A positivity-preserving and well-balanced high order compact finite difference scheme for shallow water equations*, Communications in Computational Physics, 35 (2024), pp. 524–552.
- [23] P. RIPA, *Conservation laws for primitive equations models with inhomogeneous layers*, Geophysical & Astrophysical Fluid Dynamics, 70 (1993), pp. 85–111.
- [24] M. R. SALEEM, W. ASHRAF, S. ZIA, I. ALI, AND S. QAMAR, *A kinetic flux vector splitting scheme for shallow water equations incorporating variable bottom topography and horizontal temperature gradients*, PLOS ONE, 13 (2018).
- [25] M. R. SALEEM, S. ZIA, W. ASHRAF, I. ALI, AND S. QAMAR, *The space-time CESE scheme for shallow water equations incorporating variable bottom topography and horizontal temperature gradients*, Computers & Mathematics with Applications, 75 (2018), pp. 933–956.
- [26] J. H. SEINFELD, *Atmospheric diffusion theory*, Advances in chemical engineering, 12 (1983), pp. 209–299.
- [27] C.-W. SHU, *TVB uniformly high-order schemes for conservation laws*, Mathematics of Computation, 49 (1987), pp. 105–121.
- [28] C.-W. SHU AND S. OSHER, *Efficient implementation of essentially non-oscillatory shock-capturing schemes*, Journal of Computational Physics, 77 (1988), pp. 439 – 471.
- [29] R. TOUMA AND C. KLINGENBERG, *Well-balanced central finite volume methods for the Ripa system*, Applied Numerical Mathematics, 97 (2015), pp. 42–68.
- [30] D. VANZO, A. SIVIGLIA, AND E. F. TORO, *Pollutant transport by shallow water equations on unstructured meshes: Hyperbolization of the model and numerical solution via a novel flux splitting scheme*, Journal of Computational Physics, 321 (2016), pp. 1–20.

- [31] Y. XING AND C.-W. SHU, *High order finite difference WENO schemes with the exact conservation property for the shallow water equations*, Journal of Computational Physics, 208 (2005), pp. 206–227.
- [32] Y. XING AND X. ZHANG, *Positivity-preserving well-balanced discontinuous Galerkin methods for the shallow water equations on unstructured triangular meshes*, Journal of Scientific Computing, (2013), pp. 19–41.
- [33] Z. XU AND C.-W. SHU, *Anti-diffusive finite difference WENO methods for shallow water with transport of pollutant*, Journal of Computational Mathematics, 24 (2006), pp. 239–251.
- [34] X. ZHANG, *On positivity-preserving high order discontinuous Galerkin schemes for compressible Navier–Stokes equations*, Journal of Computational Physics, 328 (2017), pp. 301–343.
- [35] X. ZHANG AND C.-W. SHU, *On maximum-principle-satisfying high order schemes for scalar conservation laws*, Journal of Computational Physics, 229 (2010), pp. 3091–3120.
- [36] X. ZHANG AND C.-W. SHU, *Maximum-principle-satisfying and positivity-preserving high-order schemes for conservation laws: Survey and new developments*, Proceedings of The Royal Society A: Mathematical, Physical and Engineering Sciences, 467 (2011), pp. 2752–2776.
- [37] J. ZHOU, D. CAUSON, C. MINGHAM, AND D. INGRAM, *The surface gradient method for the treatment of source terms in the shallow-water equations*, Journal of Computational Physics, 168 (2001), pp. 1–25.